POLICY ISSUE
INFORMATION

January 6, 2003 SECY-03-0002

FOR: The Commissioners

FROM: William D. Travers
Executive Director for Operations

SUBJECT: EVALUATION OF THE EFFECTS OF THE BALTIMORE TUNNEL FIRE ON RAIL TRANSPORTATION OF SPENT NUCLEAR FUEL

PURPOSE:

To inform the Commission of the staff's evaluation of a hypothetical event involving a spent fuel transportation cask subjected to the fire environment that occurred during the Howard Street tunnel accident in Baltimore, Maryland, in July 2001. This paper responds to the Staff Requirements Memorandum associated with COMJSM-01-0002, "Transportation of Spent Fuel."

SUMMARY:

This paper details the staff's actions related to the investigation and analysis of the Baltimore tunnel fire event that occurred in the Howard Street tunnel on July 18, 2001. The staff was tasked with assessing the consequences of this event on the transportation of spent nuclear fuel. This paper describes the following elements of the staff's actions for this investigation: the staff's coordination with the National Transportation Safety Board (NTSB) to determine the details of the train derailment and fire, the staff's technical analysis of the event, completed with assistance from the National Institute of Standards and Technology (NIST), the Center for Nuclear Waste Regulatory Analysis (CNWRA), and Pacific Northwest National Laboratory (PNNL), and the results of the staff's efforts. The staff has concluded that for a 10 CFR Part 71 approved spent fuel transportation cask subjected to the Howard Street tunnel fire, no release of radioactive materials would have resulted from this postulated event, and the health and safety of the public would have been maintained.

CONTACT: Christopher S. Bajwa, NMSS/SFPO
301-415-1237

BACKGROUND:

After the July 18, 2001, derailment of a CSX freight train inside the Howard Street tunnel in Baltimore, Maryland, the Commission directed the staff to investigate the incident and determine if current regulations for shipping spent nuclear fuel by rail are adequate to withstand the thermal conditions (i.e., flame temperature, fire duration, presence of flammable and other hazardous cargo) experienced in the tunnel. In coordination with the NTSB, and with technical assistance from NIST and the CNWRA, the staff identified the thermal conditions that were present in the tunnel during the accident.

It should be noted that although the U.S. Department of Transportation (DOT) and the U.S. Nuclear Regulatory Commission (NRC) do not have regulations requiring dedicated trains to transport spent nuclear fuel (i.e., trains shipping only spent nuclear fuel), the Association of American Railroads (AAR) has developed a performance standard for the transportation of spent nuclear fuel by rail. This performance standard dictates the use of railcars that have been analyzed and tested to minimize the possibility of derailment. Standard tanker cars used to ship flammable or hazardous materials would not meet this performance standard. Therefore, if this performance standard is followed, carriers would not ship hazardous materials on the same train as commercial spent nuclear fuel. To date, the practice in the industry has been to make spent fuel rail shipments by dedicated trains, and the industry has been self-regulating in this respect.

DISCUSSION:

The accident in the Baltimore tunnel involved a CSX freight train traveling through downtown Baltimore, Maryland. The NTSB presented details of the accident to NRC.

The Howard Street tunnel is a single-track rail tunnel, 2.7 kilometer (1.7 miles) in length, with an approximate 0.8% upward grade in the direction the train was traveling. The tunnel is constructed mostly of concrete and refractory brick. The tunnel has vertical walls and a circular ceiling and measures approximately 6.7 meters (22-feet-high) by 8.2 meters (27-feet-wide). The dimensions vary slightly along the length of the tunnel.

The CSX freight train consisted of three locomotives and 60 cars. As the train traveled through the tunnel, 11 of the 60 cars derailed. The cause of the derailment remains under investigation. A tanker railcar transporting approximately 108,263 liters (28,600 gallons) of liquid tripropylene was ruptured in the derailment and subsequently caught fire. Liquid tripropylene carries a National Fire Protection Association hazards rating of three, for flammability. This rating is the same for gasoline and signifies that tripropylene can be ignited at ambient conditions.

The freight train was also transporting tanker cars full of hydrochloric acid and other hazardous materials, which were not thought to have contributed to the fire. The precise duration of the fire is unknown.

Temperatures in the tunnel during the fire were reported (in the local media) to be as high as 815°C (1,500°F). There were indications that portions of the tunnel may have reached this temperature; however, the actual time/temperature history of the fire is not known, but has been estimated through the NIST Howard Street tunnel fire model, as described below.

ANALYSES:

The staff's consequence assessments are described in the following four sections:
1. "Event Identification"
2. "Determination of Temperatures Generated in the Howard Street Tunnel (NIST)"
3 "Confirmation of Temperatures Experienced by Materials from the Tunnel (CNWRA)"
4. "Final Staff Evaluation and Analysis of Spent Fuel Transportation Cask"

Event Identification:

The CSX train derailment accident and subsequent fire were widely reported in the media. However, detailed information was scarce. To obtain the detailed information required for the staff's analysis, on September 13, 2001, the staff met with the NTSB experts investigating this event to obtain data required for its assessments. The NTSB provided factual and photographic information of the event known at that time, such as: mechanical damage to railcars done by the derailment; fire damage to railcars; fire damage to the tunnel; and preliminary assessments of the thermal conditions in the tunnel during the fire. During the staff's meeting with the NTSB, the staff was informed that the NTSB would analyze the temperatures reached within the tunnel. However, such analyses would take time to develop. Consequently, as an interim assessment, the staff performed a scoping analysis to assess the consequences from a postulated tunnel fire event on a spent fuel transportation cask. The results of the scoping analysis were reported previously (Reference 1) and will not be discussed further.

Determination of Temperatures Generated in the Howard Street Tunnel (NIST):

Subsequent to the staff's scoping analysis, the NTSB informed the staff that it would not provide a detailed thermal analysis of the tunnel accident, as initially anticipated. The NTSB stated that since the fire was not the cause of the derailment, but a consequence of the derailment, its investigation would not quantify the temperatures reached inside the tunnel. To quantify the temperatures that existed within the tunnel, NRC contracted with NIST fire modeling experts to perform such an assessment. The results of the NIST analysis are summarized below.

Using a state-of-the-art analytic fire model, NIST calculated fire temperatures as high as 1000°C (1800°F) in the narrow flaming region of the fire. The hot gas layer above the railcars, within three rail car lengths of the fire, averaged 500°C (900°F). The tunnel surface wall temperature reached 800°C (1500°F) where the fire directly impinged on the top of the tunnel. The average tunnel ceiling temperature, within a distance of three rail cars from the fire, was 400°C (750°F).

To obtain confidence in the results calculated by NIST, the analytic models were validated against data taken from a series of fire experiments conducted in an abandoned West Virginia highway tunnel. The data were part of the Memorial Tunnel Fire Ventilation Test Program performed by the Federal Highway Administration and Parsons Brinckerhoff, Inc.

The internal NIST report documenting the fire analysis is provided as Attachment 1 to this paper. This report will be issued as NUREG/CR-6793 upon completion of printing.

Confirmation of Temperatures Experienced by Materials from the Tunnel (CNWRA):

As an added validation of the fire analyses performed by NIST experts, the staff contracted with CNWRA experts in fire testing, fire modeling, and materials analysis, to examine the physical properties of the paint and metals from the rail cars (box cars and tanker cars) removed from the tunnel after the fire. To determine the time and temperature exposure of these samples, metallurgical analyses were performed on several different materials, including sections of the boxcars exposed to the most severe portion of the fire, as well as an air brake valve from the tripropylene tanker car. The CNWRA analyses confirmed the temperatures calculated by NIST as consistent with the conditions observed in the paint and metals. The CNWRA report on its analysis is provided as Attachment 2 to this paper.

Final Staff Evaluation and Analysis of Spent Fuel Transportation Cask:

The NRC staff, with the assistance of thermal analysis experts at PNNL, developed a refined 2-dimensional finite element analysis thermal model of the transportation cask, including the transport cradle. The purpose of the refined model was to perform a more realistic thermal assessment that captured the non-uniform temperature distributions which existed in the Howard Street tunnel fire. The staff imposed both temperature and flow boundary conditions derived by NIST for the Howard Street tunnel fire to the spent fuel cask analytic model. The staff examined two scenarios in the cask thermal response analysis.

The first scenario was based on the DOT regulations that require railcars carrying radioactive materials be separated by at least one railcar (known as a buffer car) from hazardous materials or flammable liquids. The staff's analysis assumed one railcar [20 meters (65.6 feet)] separation between the spent fuel cask and the fire source. The staff applied a boundary condition, based on the NIST analysis, onto the cask in three "zones." The upper third of the cask was conservatively exposed to the maximum temperatures and flow that existed in the upper portion of the tunnel; the middle third of the cask was conservatively exposed to the maximum temperatures and flow that existed along the side of the tunnel; and the bottom third of the cask, including the shipping cradle, was conservatively exposed to the maximum temperature and flow conditions along the lower elevations of the tunnel. The cask model accounts for the effects of radiation from the tunnel walls and the effects of the mounting cradle which secures the transportation cask to a specially designed railcar.

The second scenario placed the cask 5 meters (16.4 feet) from the fire source. This scenario was considered a bounding scenario, since it is unlikely that a spent fuel transportation cask, if one had been involved in the Howard Street tunnel derailment and fire, would have been adjacent to the fuel source.

Both scenarios were calculated through 150 hours of fire exposure (i.e., the fire was assumed to burn at the maximum temperatures calculated for the 150 hour duration). Note that the liquid tripropylene fuel burned for about 3 hours in the actual Howard Street tunnel fire, and the tripropylene tank car held enough fuel for a burn time of 6 to 7 hours based on a 9 meter pool diameter.

For the 20-meter (65.62-feet) scenario, the analysis indicated that the short-term temperature limit of the Zircalloy fuel cladding, 570°C (1058°F), would have been exceeded 116 hours into

the fire exposure. For the 5-meter (16.4-feet) scenario, the fuel cladding temperature limit would have been exceeded at 37 hours into the fire exposure. The short-term temperature limit is a conservative regulatory tool used to ensure no fuel rod cladding breach. It is not a temperature limit that implies gross rupture of fuel cladding. Additional calculations were performed to determine stresses that resulted from the fire in the welded multipurpose canister (MPC) that provides the primary boundary to release of radioactive materials. The stress calculations indicated that the MPC would not fail during the fire, and thus there would be no radioactive release for the analyzed event.

The staff also examined the risk of radioactive doses to first responders after a severe fire accident. Since the cask's polymeric neutron shield would be damaged under severe fire conditions, the magnitude of the neutron field would increase in the vicinity of the cask. This assessment is accounted for in staff's review of the HOLTEC HI-STAR cask application under 10 CFR 71.73, where the neutron shield was assumed to be consumed during the hypothetical accident condition fire. The licensing analyses for this cask demonstrated that without the neutron shield, the post-accident dose rates would be within the limits prescribed in 10 CFR 71.51. Therefore, the complete loss of the neutron shield does not pose a risk to the health of the public outside of those allowed by NRC regulations.

CONCLUSION:

The staff's assessment of the hypothetical event of a spent nuclear fuel transportation cask in the Howard Street tunnel fire environment identified no public health and safety concerns. The staff's analyses indicated no failure of the structural components of the transport cask nor failure of the canister containing the spent fuel inside the transportation cask. The refined cask analysis described above confirmed the existence of significant conservatism in the staff's preliminary scoping analysis. Consequently, the staff concluded that there would be no release of radioactive materials from this postulated event and that existing programs provide reasonable assurance of adequate protection to the public.

REFERENCES:

1. "An Analysis of a Spent Fuel Transportation Cask Under Severe Fire Accident Conditions." Chris Bajwa. ASME pressure Vessel and Piping Conference Proceedings. August, 2002. (ADAMS Accession #ML021690392)

/RA/

William D. Travers
Executive Director
for Operations

Attachments: 1. Internal NIST Report
2. CNWRA Report

NISTIR 6902

Numerical Simulation of the Howard Street Tunnel Fire, Baltimore, Maryland, July 2001

Kevin B. McGrattan
Anthony Hamins

NIST National Institute of Standards and Technology • Technology Administration • U.S. Department of Commerce

NISTIR 6902

Numerical Simulation of the Howard Street Tunnel Fire, Baltimore, Maryland, July 2001

Kevin B. McGrattan
Anthony Hamins
Fire Research Division
Building and Fire Research Laboratory

August 2002

U.S. Department of Commerce
Donald L. Evans, Secretary

National Institute of Standards and Technology
Arden L. Bement, Director

Abstract

This report documents a study undertaken to estimate the thermal environment of the Howard Street Tunnel in Baltimore, Maryland, following the derailment in July 2001 of a freight train and the burning of spilled tripropylene and the contents of surrounding rail cars. A numerical fire model developed by the National Institute of Standards and Technology (NIST) has been used to simulate the fire's growth and spread in the tunnel. The fire model has been validated for this application using temperature data collected during a series of fire experiments conducted at a decommissioned highway tunnel in West Virginia. The cross-sectional area of the tunnel and the fire sizes used in the West Virginia experiments are similar to the Howard Street Tunnel.

For the Howard Street Tunnel fire, the peak calculated temperatures within the tunnel were approximately 1,000 °C (1,800 °F) within the flaming regions, and on average approximately 500 °C (900 °F) when averaged over a length of the tunnel equal to three to four rail car lengths. Because of the insulation provided by the thick brick walls of the tunnel, the calculated temperatures within a few car lengths of the fire were relatively uniform, consistent with what one would expect to find in an oven or furnace. The peak wall surface temperature reached about 800 °C (1,500 °F) where the flames were directly impinging, and on average 400 °C (750 °F) over the length of three to four rail cars. The steel temperature of the rail cars would be expected to be similar to the surrounding gas temperature because of the long exposure time and the high thermal conductivity of steel.

Contents

Abstract **iii**

1 Introduction **1**

2 Technical Approach **2**

3 Model Validation Studies **4**
3.1 Fire Model Evaluation for Nuclear Power Plant Applications 4
3.2 Memorial Tunnel Fire Ventilation Test Program 8

4 Howard Street Tunnel Fire Simulation Parameters **14**

5 Calculation Results **19**

6 Analysis and Discussion **22**
6.1 Burning Rate 22
6.2 Parameter Study 26

7 Conclusion **28**

A Numerical Method **31**
A.1 Conservation Equations 31
A.2 Combustion 32
A.3 Thermal Radiation 35
A.4 Convective Heat Transfer to Walls 36

List of Figures

1 Geometry of the fire test hall used in the validation study 5
2 Comparison of measured and predicted temperatures for a fire in a 19 m tall test hall 7
3 Cross section of Memorial Tunnel, West Virginia 9
4 Temperatures after 5 minutes for the 20 MW unventilated fire test performed as part of the Memorial Tunnel Fire Ventilation Test Program 10
5 Temperatures after 16 minutes for the 20 MW unventilated fire test performed as part of the Memorial Tunnel Fire Ventilation Test Program 11
6 Temperatures after 3 minutes for the 50 MW unventilated fire test performed as part of the Memorial Tunnel Fire Ventilation Test Program 12
7 Temperatures after 14 minutes for the 50 MW unventilated fire test performed as part of the Memorial Tunnel Fire Ventilation Test Program 13
8 Sketch of Howard Street Tunnel and derailed cars 15
9 Elevation diagram of Howard Street Tunnel 16
10 Predicted temperatures along the centerline vertical plane at 5 and 30 min after ignition of the Howard Street Tunnel fire 20
11 Predicted oxygen concentration along the centerline vertical plane at 5 and 30 min after ignition of the Howard Street Tunnel fire 21
12 Schematic diagram showing how smoke and fresh air mix within a tunnel 22
13 Box car pulled from the Howard Street Tunnel 23
14 Tripropylene tank car after the fire 24
15 Right side of car #53, a tank car carrying hydrochloric acid 25
16 State relations for nonene 34

1 Introduction

On July 18, 2001, at 3:08 pm, a 60 car CSX freight train powered by 3 locomotives traveling through the Howard Street Tunnel in Baltimore, Maryland, derailed 11 cars. A fire started shortly after the derailment. The tunnel is 2,650 m (8,700 ft, 1.65 mi) long with a 0.8 % upgrade in the section of the tunnel where the fire occurred. There is a single track within the tunnel. Its lower entrance (Camden portal) is near Orioles Park at Camden Yards; its upper entrance is at Mount Royal Station. The train was traveling towards the Mount Royal portal when it derailed. For almost its entire length the tunnel runs beneath Howard Street. A fire erupted under the intersection of Howard and Lombard Streets where a ruptured tank car (52nd out of 60 cars) spilled tripropylene onto the floor of the tunnel. It is unclear how the fire started, but it is speculated that a spark produced when the tank car was punctured could have been the cause. The liquid fuel sustained a fire that lasted several hours. It is believed that other materials burned slowly for several days within closed box cars. The other cars on the train were transporting a variety of bulk materials including pulp board, brick, steel, soy oil, paper, and a variety of corrosive acids.

Under the sponsorship of the US Nuclear Regulatory Commission (NRC), the Building and Fire Research Laboratory of the National Institute of Standards and Technology (NIST) has undertaken a study of the incident to assess the thermal environment within the tunnel during the fire. The National Transportation Safety Board (NTSB) has conducted an investigation of the tunnel fire and provided NIST with information about the tunnel, the damage to the rail cars, and various other details [1]. Using information collected at the scene by the NTSB, a series of numerical simulations has been performed to predict the temperature of the hot gases and the heat flux to various objects within the tunnel.

The simulations reported in this study are not intended to replicate every detail of the Howard Street Tunnel fire, since the information about the fuel spill, tunnel floor, track and ballast, *etc.*, is not known to a high enough level of certainty to permit an exact reconstruction of the event. The approach taken is to use what information is known about the incident as a starting point for the calculations, and then to vary the unknown parameters to ascertain the range in possible outcomes. This information is useful in assessing the risk to materials that are commonly transported by rail.

2 Technical Approach

In cooperation with the fire protection engineering community, a numerical fire model, Fire Dynamics Simulator (FDS), is being developed at NIST to study fire behavior and to evaluate the performance of fire protection systems in buildings. Version 2 of FDS was publicly released in December 2001 [2, 3]. The model is based on the low Mach number form of the Navier-Stokes equations and uses a large eddy simulation (LES) technique to represent unresolved, sub-grid scale motion. The fire is modeled by solving a transport equation for the conserved scalar quantity known as the mixture fraction, a linear combination of the fuel and oxygen that indicates the mass fraction of the gas originating as fuel. The advantage of the mixture fraction approach is that all of the species transport equations are combined into one, reducing the computational cost. Thermal radiation is modeled by solving the radiative transport equation for a non-scattering gray gas using what is known as the Finite Volume Method [4].

Improvements have been made to FDS version 2 to extend its range of application to include the long tunnel geometry and the under-ventilated fire conditions. The most important improvement for this problem is the addition of a multiblock meshing scheme. Originally, the FDS algorithm solved the fluid dynamic equations on a single rectangular uniform mesh that spanned the volume of interest. The problem with this approach is that too much computational time is wasted in regions that do not necessarily require high resolution. For example, when simulating the fire and smoke movement in a long tunnel, only the region near the fire needs to be covered with a fine numerical grid. The rest of the tunnel need not have such a fine grid. The use of multiple numerical grids of various spatial sizes allows the computational domain to be extended to accommodate the entire length of the tunnel, but still retain high accuracy near the fire.

The calculations to be discussed solve the mass, momentum and energy conservation equations on a computational grid whose cells are on the order of 15 cm to 30 cm (6 in to 1 ft) near the fire source. A coarse mesh is used farther from the fire where it is not as important to capture the detailed mixing of fuel and oxygen. The objective of the calculations is to estimate the temperatures within the tunnel, and the heat flux to surrounding objects. As a check on the numerical algorithm, several fire experiments for which temperature measurements are available have been simulated first to ensure that the numerical model is working properly, and that the chosen numerical grid is adequate.

FDS can provide valuable insight into how a fire may have developed. The model, however, is only a simulation. The model output is dependent on a variety of input values such as material properties, timelines, geometry, and ventilation openings. Since perfect knowledge of every detail of the fire site, fuel load or timeline is never known, estimations are incorporated into the model. To better understand the sensitivity of modeling results to variation of these parameters, a parametric study using FDS was performed. For example, a parametric study was conducted on the effect of the thermal conductivity of the bricks lining the tunnel, the size of the fuel spill, and the effect of the tunnel dimensions. These parametric studies are described in Section 6 of this report.

The ability of the FDS model to accurately predict the temperature and velocity of fire gases has been previously evaluated by conducting experiments, both lab-scale and full-scale, and measuring quantities of interest. For relatively simple fire-driven flows, such as buoyant plumes and flows through doorways, FDS predictions are within the experimental uncertainty of the values measured in the experiments [5]. In large-scale fire tests reported in Ref. [6], FDS temperature predictions were found to be within 15 % of the measured temperatures and the heat release rates

were within 20 % of the measured values. In full-scale tunnel fire tests, FDS simulations were within 50 °C (100 °F) of the peak measured values. The results in this report are presented as ranges to accommodate the uncertainties.

Further details on the numerical model may be found in the Appendix. A complete description of the numerical model can be found at the web site

`http://fire.nist.gov/fds`

3 Model Validation Studies

Two sets of calculations are included in this section to demonstrate the capabilities of the FDS model. The first set of calculations was performed to validate the model's ability to predict the movement of smoke and hot gases from a fire in a relatively large, open building. They are included here as an example of how the model is often used in practice by fire protection engineers. The FDS model is used by hundreds of engineers around the world, who constantly validate it for use in a wide variety of problems. These validation exercises raise the level of confidence in applying the model to fire scenarios that are different from those commonly seen in residential or industrial settings.

The geometry of the second validation exercise is directly related to the present study. It compares calculations to measurements for a set of fire experiments performed in a decommissioned highway tunnel in West Virginia. Although the tunnel is slightly larger in cross section than the Howard Street Tunnel, the temperatures measured during these experiments should not be significantly different from those experienced during the Howard Street Tunnel fire, and provide a useful check on the simulations to be performed for the current study.

3.1 Fire Model Evaluation for Nuclear Power Plant Applications

FDS has recently been applied to a series of benchmark fire tests performed as part of the *International Collaborative Project to Evaluate Fire Models for Nuclear Power Plant Applications* [7]. The tests analyzed were designated as Benchmark Exercise #2. Three fire experiments were performed in a large fire test hall. In each, a pool of heptane was burned for about 5 minutes, during which time gas temperatures were measured in three vertical arrays and at two points within the fire plume. The hall was 27 m (89 ft) long, 14 m (45 ft) wide and 19 m (62 ft) high with a sloped ceiling, an exhaust duct, and several doors opening near its base. The fire size and ventilation configurations were changed from test to test.

Figure 1 shows the geometry of the test hall and the layout of the various numerical grids used in the simulation. The finest grid surrounding the fire is 4 m by 4 m by 10 m high, with grid cells 13 cm on a side. Five other separate grids are used to cover the rest of the space at a resolution of 40 cm. Within each grid, the cells are uniform in size. In all, 216,000 grid cells are used in the calculation. Ten minutes of real time are simulated. Some simplifications to the geometry include making the burner and the exhaust duct square rather than round, and approximating the sloped ceiling as a series of stair steps. Because boundary layer effects were not considered important, these approximations did not impact the final results. Otherwise, everything else is as specified in the problem description. Heptane (C_7H_{16}) is used as a fuel. Temperature and velocity predictions are recorded at all of the specified locations.

The results of the calculations agree well with the measurements. An example of the results is shown in Fig. 2. The predicted temperatures at the 5 upper thermocouple locations in each array are within 10 °C of the measured temperatures, which are 100 to 150 °C above ambient. The lower 5 temperature locations show good agreement as well, with the greatest difference being for the lowest thermocouple, which under-predicts the measured temperatures by about 10 °C. The measured temperatures in the lower layer were 20 to 100 °C above ambient. Given slightly higher temperatures in the upper layer, it is not surprising to see slightly lower temperatures somewhere else since the model conserves energy. The model assumes that there is no air movement in the

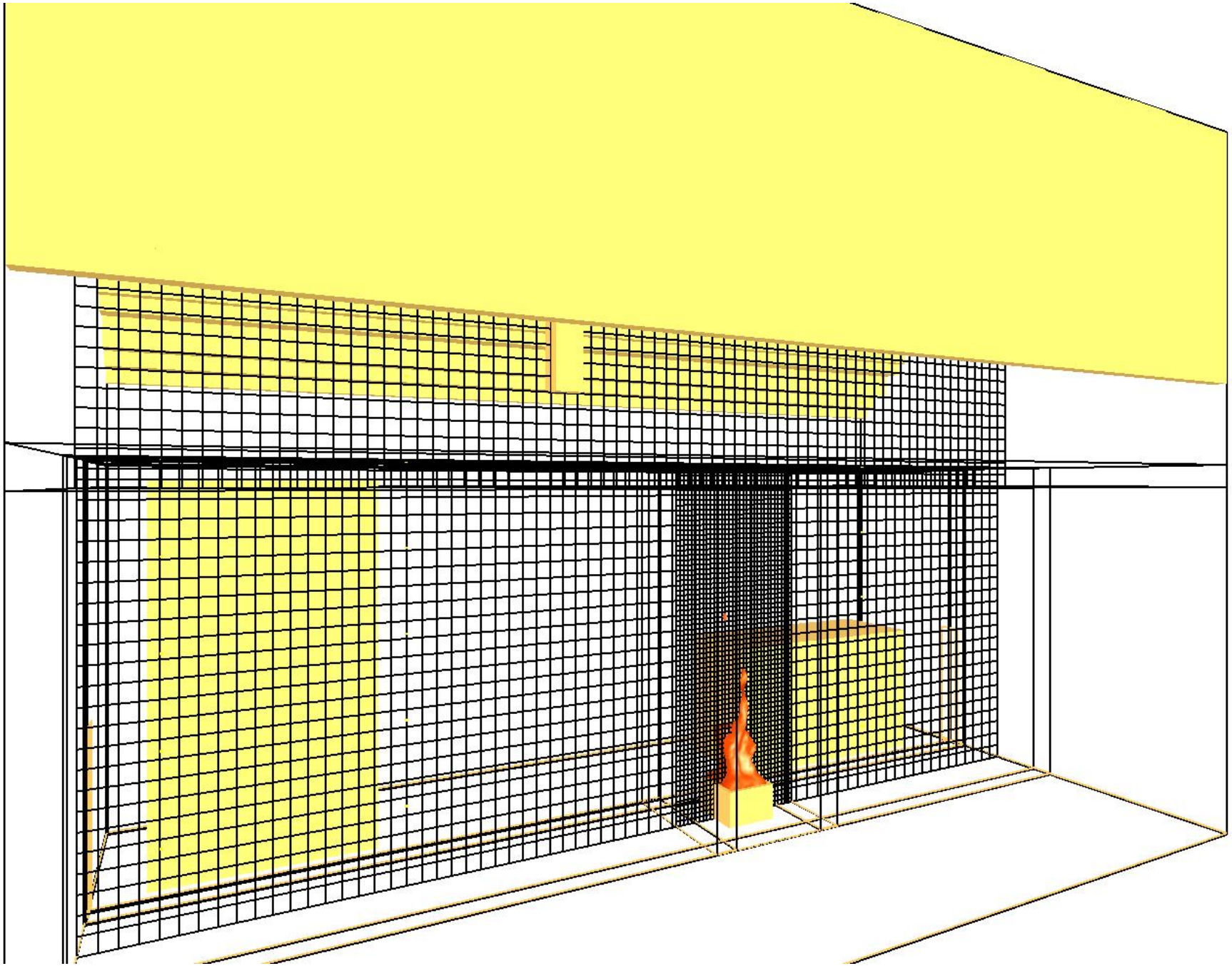

FIGURE 1: Geometry of the fire test hall used in the validation study, showing the various numerical grids used in the calculations.

hall except for that induced by the fire or the ventilation system, thus one would expect the level of mixing to be slightly under-predicted. Another source of uncertainty in the measurement is the absorption of thermal radiation by the thermocouples in the lower layer, leading to slightly higher thermocouple temperatures over the surrounding gas temperature.

The results of this exercise are very favorable. The numerical model works very well in situations where the heat release rate is known, and the fire has an adequate supply of oxygen, as in these tests. When the heat release rate is not known, and when the fire is not free to burn at its peak rate because of oxygen limitations, the results are subject to greater uncertainty, as in the next example.

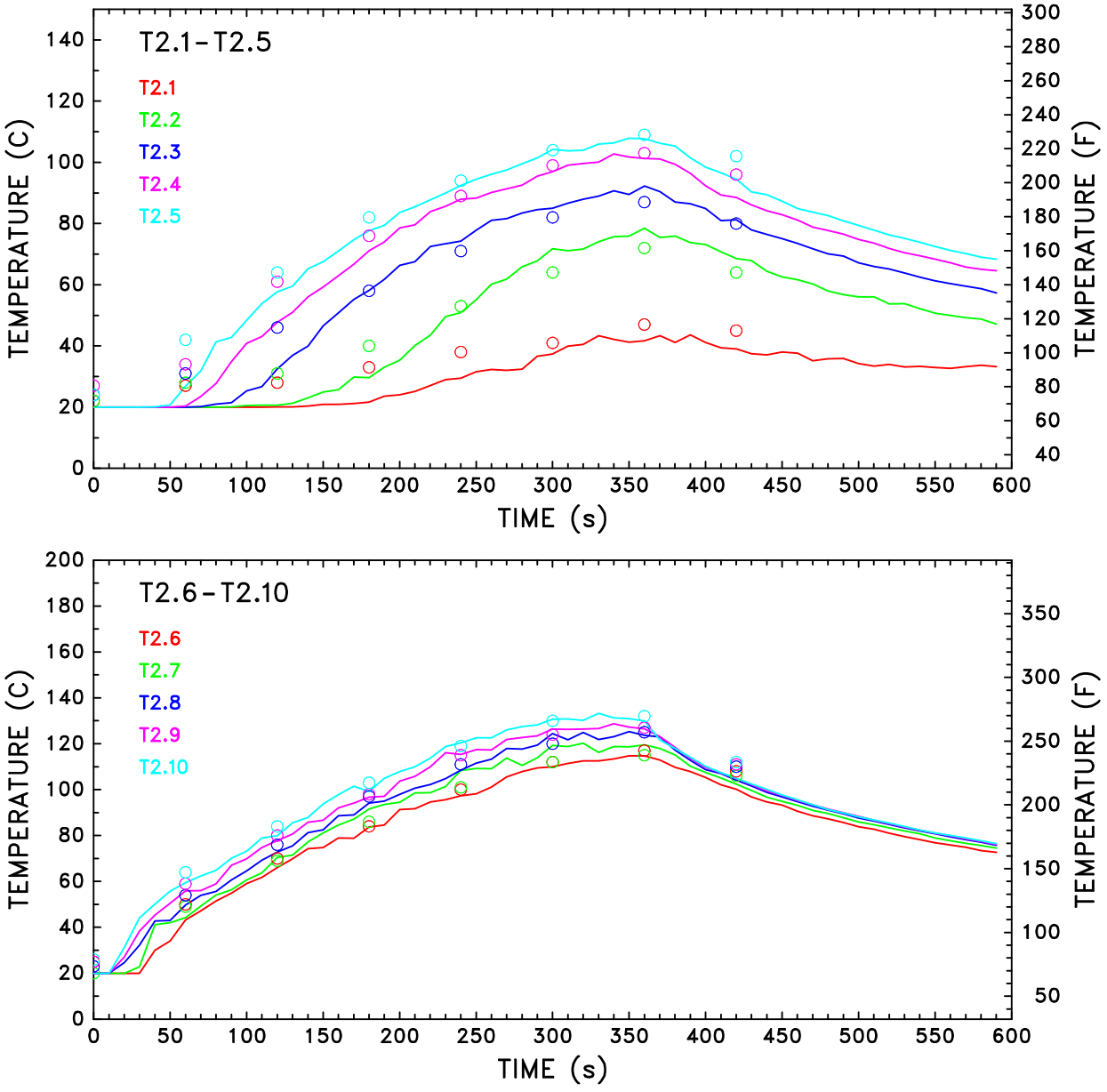

FIGURE 2: Comparison of measured (circles) and predicted (lines) temperatures along a vertical rake of thermocouples in the center of a 19 m tall test hall. The peak heat release rate for the 10 min test was 3.8 MW. The thermocouples labeled T2.1 to T2.10 span the height of the hall from 2 m off the floor to 1 m below the ceiling.

3.2 Memorial Tunnel Fire Ventilation Test Program

The second validation exercise of the model involves one of a series of tunnel fire experiments conducted in a decommissioned highway tunnel in West Virginia from 1993 to 1995 [8]. The tunnel is 853 m (2,800 ft) long with a 7.9 m (26 ft) ceiling height, a 3.2 % upgrade, and a semi-circular ceiling (see Fig. 3). A series of fire tests was conducted by Parsons Brinckerhoff in which various fire sizes and ventilation schemes were used. Of most relevance to the Howard Street Tunnel fire were tests with fire sizes of 20 MW and 50 MW and only natural ventilation. The fuel for the tests was No. 2 fuel oil poured on top of water in large pans. The fuel surface was about 0.6 m (2 ft) off the floor of the tunnel. The burning rate of fuel was not monitored during the tests. Instead, the pan size was chosen so that the burning rate would be approximately what was desired based on previously measured burning rates of the fuel.

The temperatures recorded near the ceiling of the tunnel directly over the fire during the 20 MW and 50 MW tests are considerably different. For the 20 MW test, the gas temperature over the fire reached approximately 300 °C (600 °F), whereas for the 50 MW test, the temperature reached approximately 800 °C (1,500 °F) during the 15 min burn period. The measured temperatures within the fire itself were similar in both tests.

For the 20 MW fire, Figures 4 and 5 show temperature contours along a vertical centerline plane at times of 5 min and 16 min past ignition of the fuel for both the experiments and the simulations. The tunnel has a 3.2 % upgrade (Howard Street Tunnel has a 0.8 % upgrade), which accounts for the smoke and heat moving to the left (uphill). Peak temperatures above the fire were measured to be about 320 °C (600 °F). The numerical simulation was conducted with a numerical grid whose cells are on the order of 30 cm (1 ft) for covering a 130 m (425 ft) section of the tunnel surrounding the fire pan. The peak temperatures agree to within 50 °C (100 °F). At the uphill end of the tunnel, the simulation under-estimates the extent of the lower temperature contours. For example, in Fig. 5, the 200 °F contour extends half way to the Fan Room over the left opening of the tunnel, whereas in the numerical simulation, this same temperature contour only extends about a quarter of the way. The reason for this difference is that the simulation employs coarser numerical grids at the ends of the tunnel since the objective of the calculations is to predict the thermal environment within 100 m of the fire.

For the 50 MW fire, Figures 6 and 7 show temperature contours along a vertical centerline plane at times of 3 and 14 minutes past ignition of the fuel for both the experiments and the simulations. Peak temperatures above the fire were measured to be about 800 °C (1,500 °F) in the first few minutes, decreasing to about 700 °C (1,300 °F) after 14 min. The slight reduction in peak temperatures most likely is due to the underventilated environment in the upper layer of the tunnel which restricts the fuel from burning close to the ceiling. In the numerical simulation, the peak temperature is within 50 °C (100 °F) of the experimental measurement. At the uphill end of the tunnel, the simulation under-estimates the extent of the lower temperature contours. For example, in Fig. 7, the 200 °F contour extends to the Fan Room over the left opening of the tunnel, whereas in the numerical simulation, this same temperature contour only extends about two-thirds of the way. The reason for this difference is that the simulation employs coarser numerical grids at the ends of the tunnel since the objective of the calculations is to predict with as much accuracy as possible the thermal environment within 100 m of the fire.

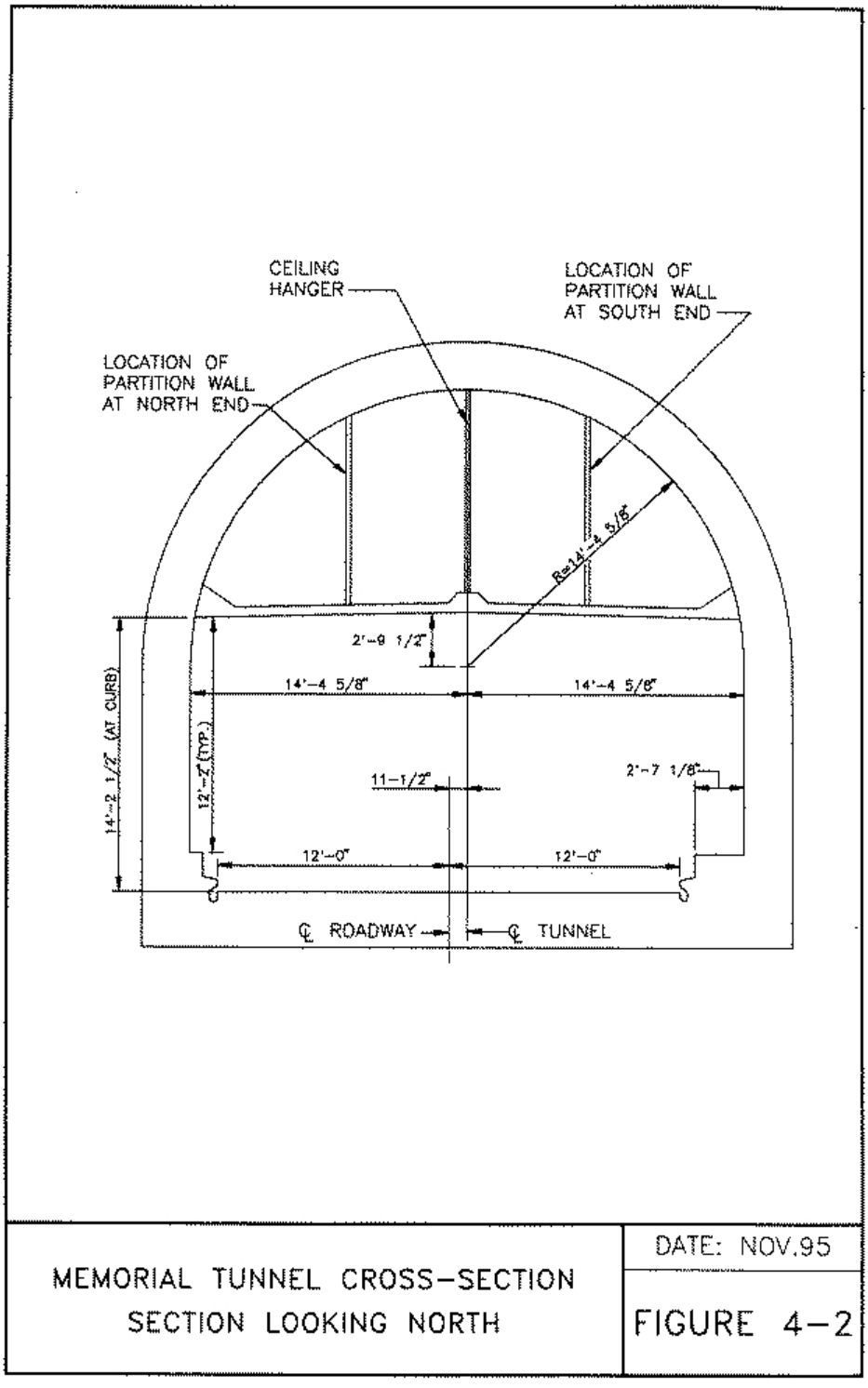

FIGURE 3: Cross section of Memorial Tunnel, West Virginia, reprinted from Reference [8]. Note that all lengths are reported in units of feet and inches. The height of the tunnel is 7.9 m (26 ft); its width is 8.8 m (29 ft). The tunnel walls and ceiling are constructed of concrete. In comparison, the Howard Street Tunnel in Baltimore is approximately 6.7 m (22 ft) high, 8.2 m (27 ft) wide, and lined with brick.

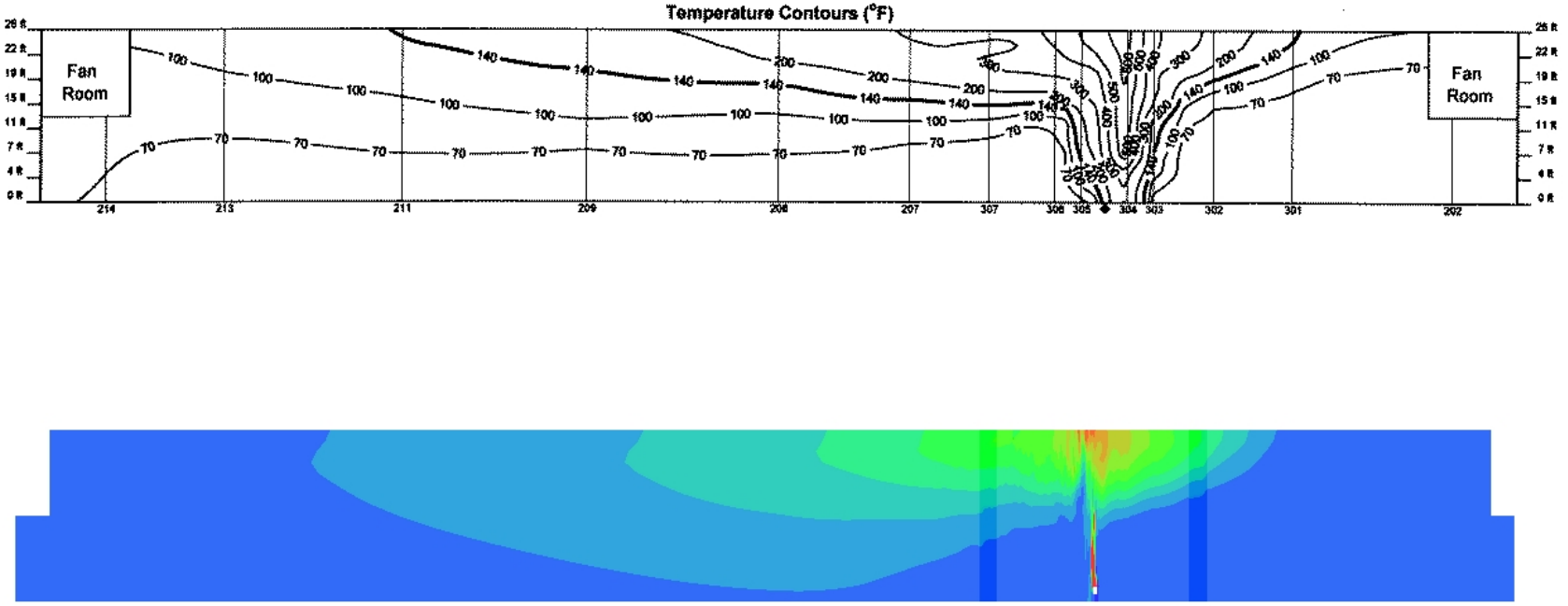

FIGURE 4: Temperatures along the centerline vertical plane during the 20 MW unventilated fire test performed as part of the Memorial Tunnel Fire Ventilation Test Program. Shown are the experimental (top figure) and predicted (lower figure) temperatures 5 minutes past ignition. The colored contours in the lower figure are at increments of 60 °F, starting at 60 °F which separates the light and dark blue regions. The red contours in the lower figure denote regions in excess of 300 °C (600 °F). The highest temperature contour in the upper figure is 600 °F over the fire near the ceiling. The tunnel is not shown to scale. The tunnel slopes upwards from right to left.

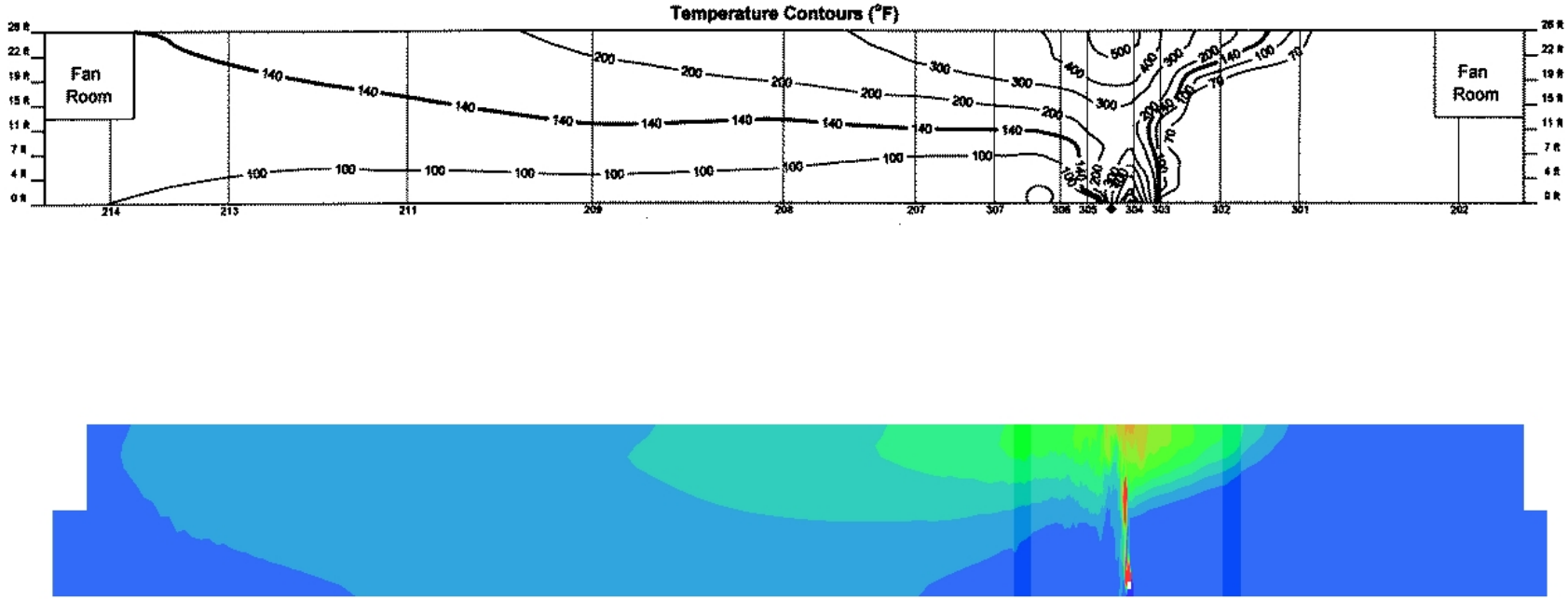

FIGURE 5: Temperatures along the centerline vertical plane during the 20 MW unventilated fire test performed as part of the Memorial Tunnel Fire Ventilation Test Program. Shown are the experimental (upper figure) and predicted (lower figure) temperatures 16 minutes past ignition. The colored contours are at increments of 60 °F, starting at 60 °F which separates the light and dark blue regions. The red contours in the lower figure denote regions in excess of 300 °C (600 °F). The highest temperature contour in the upper figure is 500 °F. The tunnel is not shown to scale. The tunnel slopes upwards from right to left.

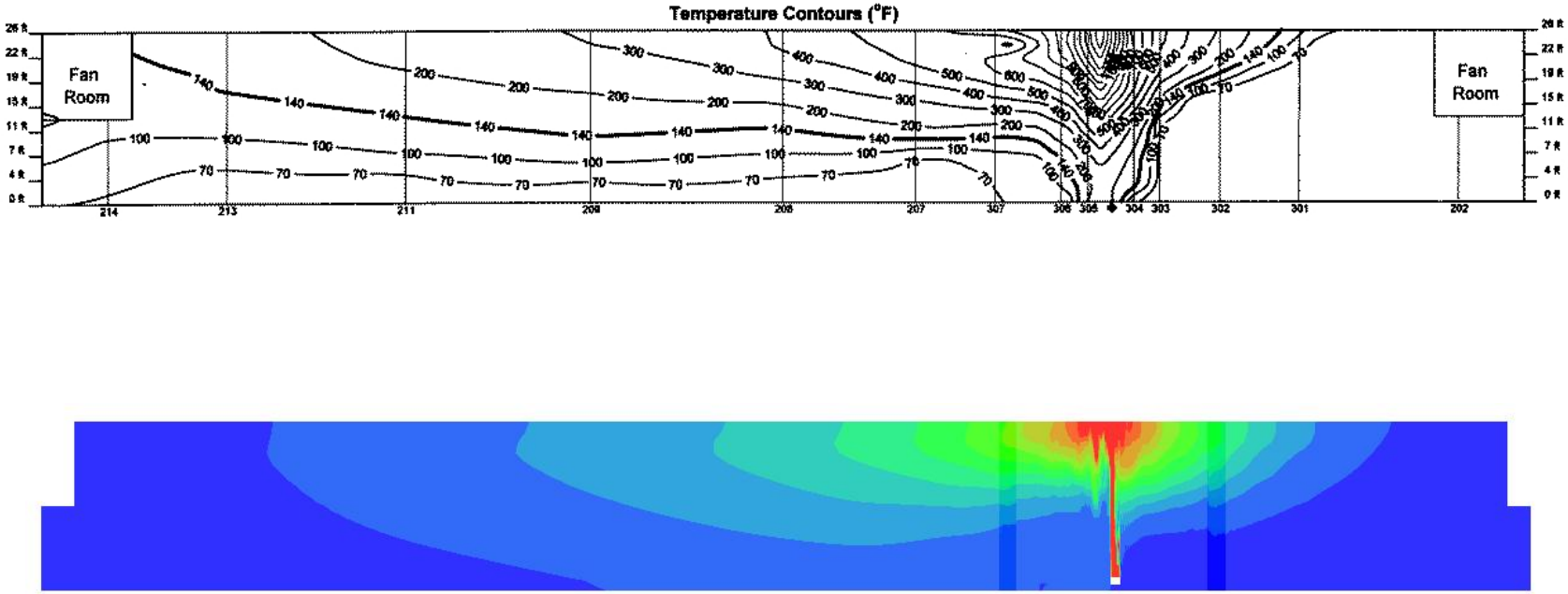

FIGURE 6: Temperatures along the centerline vertical plane during the 50 MW unventilated fire test performed as part of the Memorial Tunnel Fire Ventilation Test Program. Shown are the experimental (upper figure) and predicted (lower figure) temperatures 3 minutes past ignition. The colored contours are at increments of 100 °F, starting at 100 °F which separates the light and dark blue regions. The red contours in the lower figure denote regions in excess of 600 °C (1,100 °F). The highest predicted temperature is 750 °C (1,400 °F). The highest temperature contour in the upper figure is 1,500 °F. The tunnel is not shown to scale. The tunnel slopes upwards from right to left.

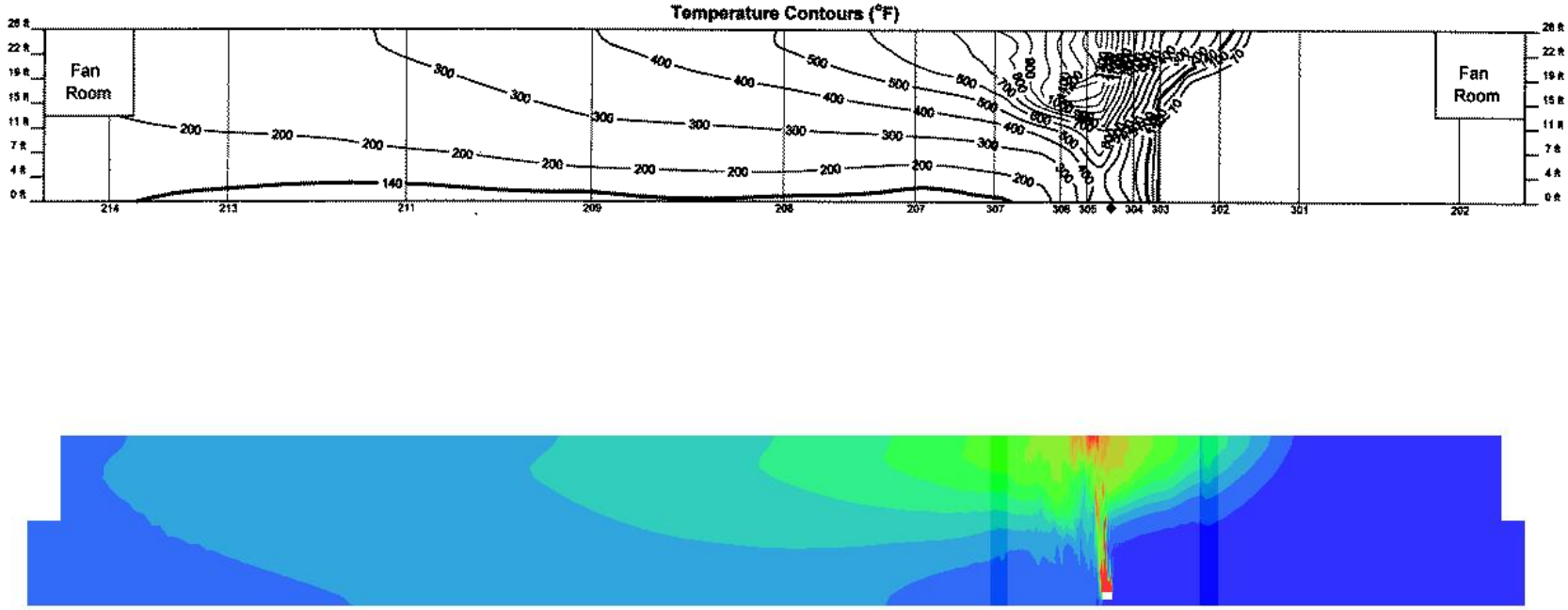

FIGURE 7: Temperatures along the centerline vertical plane during the 50 MW unventilated fire test performed as part of the Memorial Tunnel Fire Ventilation Test Program. Shown are the experimental (upper figure) and predicted (lower figure) temperatures 14 minutes past ignition. The colored contours are at increments of 100 °F, starting at 100 °F which separates the light and dark blue regions. The red contours in the lower figure denote regions in excess of 600 °C (1,100 °F). The peak predicted temperature is 700 °C (1,300°F). The highest experimental temperature contour is 1,300 °F. The tunnel is not shown to scale. The tunnel slopes upwards from right to left.

4 Howard Street Tunnel Fire Simulation Parameters

The comparison of the Memorial Tunnel Fire Test results with those of FDS supports the use of the model for the Howard Street Tunnel fire. In this section, we will discuss the various model inputs, with an emphasis on the similarities and differences between the Howard Street and Memorial Tunnel fires. Information about the accident has been provided by the National Transportation Safety Board in the form of photographs of the scene and sketches of the tunnels, Figs. 8 and 9.[1]

The overall geometry of the Memorial and Howard Street Tunnels is similar. Because of this, it is expected that the fire behavior in both would be similar. Both have barrel-shaped roofs, both are relatively small in cross-sectional area. The height of the Memorial Tunnel is 7.9 m (26 ft); its width is 8.8 m (29 ft). In comparison, the Howard Street Tunnel is approximately 6.7 m (22 ft) high, 8.2 m (27 ft) wide, although these dimensions vary over the length of the tunnel. In the vicinity of the fire, the Howard Street Tunnel is 6.4 m (21.0 ft) high and 9.9 m (32.5 ft) wide. The Memorial Tunnel is 850 m (2,800 ft, 0.53 mi) long, whereas the Howard Street Tunnel is 2,650 m (8,700 ft, 1.65 mi) long. The Memorial Tunnel has a 3.2 % upgrade; the Howard Street Tunnel has a 0.8 % upgrade in the section of the tunnel where the fire occurred. The 0.8 % upgrade persists until the Mount Royal portal (see Fig. 9).

The rail cars in the tunnel were assumed to be solid blocks 3.0 m (10 ft) wide and 4.0 m (13 ft) high with 1.0 m (3 ft) of void space beneath to represent the undercarriage. Most of the cars were centered in the tunnel, but several of the derailed cars were offset based on the diagram of the accident scene provided by the NTSB. The cars in the simulation served as targets of thermal radiation and obstructions limiting the airflow to the fire. Specific damage to the cars was not included in the simulations.

The fire in the Howard Street Tunnel is believed to have been fueled initially by spilled tripropylene. This liquid is assumed to consist mainly of nonene (C_9H_{18}, relative molecular mass 126 g/mol). Ideally, nonene burns according to the reaction

$$2\ C_9H_{18} + 27\ O_2 \rightarrow 18\ CO_2 + 18\ H_2O \tag{1}$$

The heat of combustion for the reaction is ideally 44,300 kJ/kg, but is less in under-ventilated environments, where the production of soot and CO (among many other by-products of incomplete combustion) is substantial. Measurements of the exhaust gases from fully-involved room fire experiments show that the yields[2] of soot and CO are on the order of 0.2, although no data are available specifically for tripropylene/nonene [9]. The conversion of the carbon in the fuel into soot and CO, rather than CO_2, reduces the heat of combustion from its ideal value.

The pool of tripropylene was assumed to evaporate with a heat of vaporization of 300 kJ/kg and a boiling temperature of 135 °C [10]. The calculations were relatively insensitive to the exact value of these parameters because the fire was oxygen-limited. In other words, the fuel evaporated readily in the hot tunnel; there was more fuel vapor than there was oxygen to burn it. Changing the heat of vaporization and boiling temperature had little effect on the final results. More discussion of these types of parameter sensitivities can be found in the Analysis and Discussion (Section 6).

The tunnel was assumed to be lined with a meter-thick layer of brick. The number of courses (layers) of brick varied between 8 (36 in, 0.9 m) in the vicinity of the fire, and 5 (22.5 in, 0.6 m)

[1] These sketches may be difficult to read in printed form. The electronic version of the report contains the original images that can be enlarged to show detail.

[2] The *yield* of a combustion product is the mass of the product produced per unit mass of fuel burned

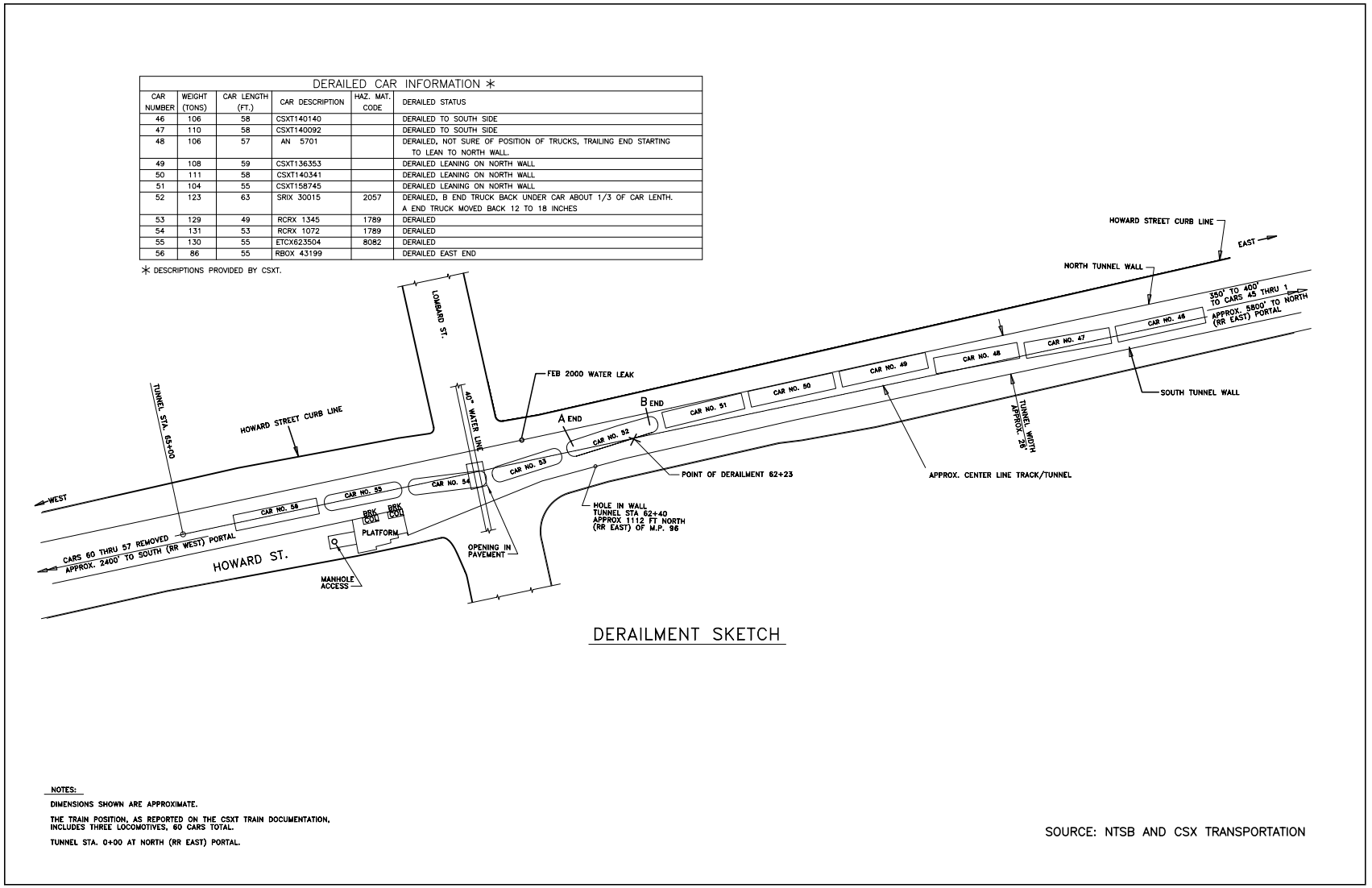

FIGURE 8: Sketch of Howard Street Tunnel and derailed cars, courtesy of the National Transportation Safety Board.

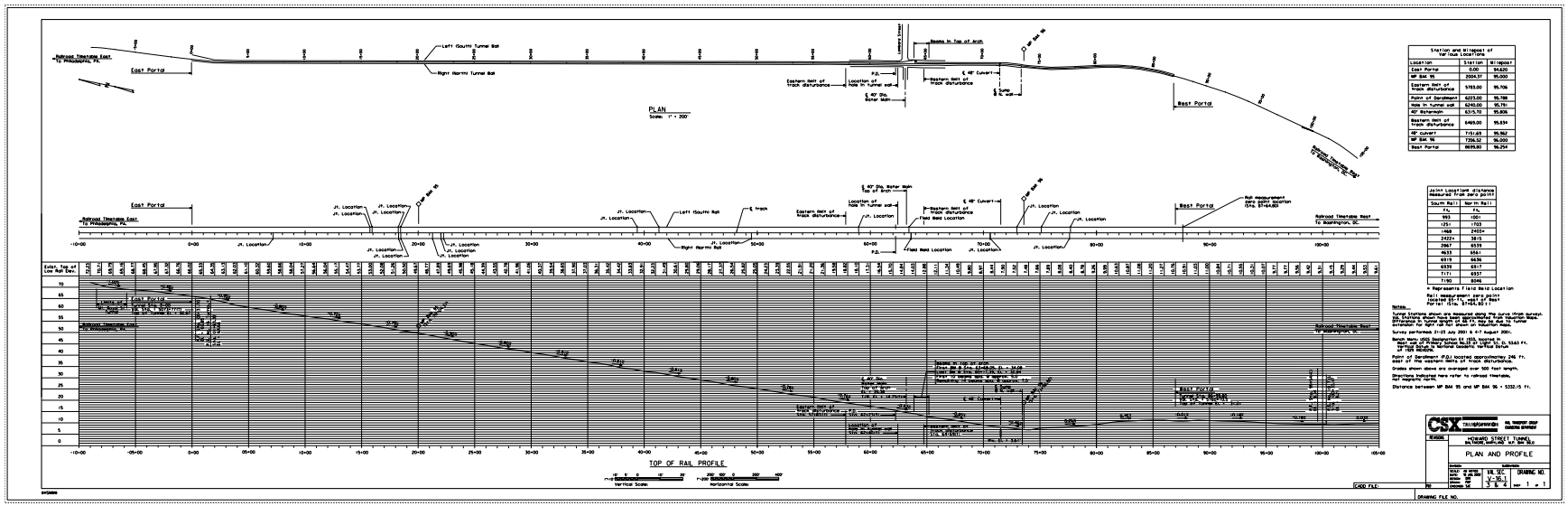

FIGURE 9: Elevation diagram of Howard Street Tunnel, courtesy of the National Transportation Safety Board.

towards the Mount Royal portal. The properties of the brick were assumed as follows: thermal conductivity 0.7 W/(m·K), specific heat 835 J/(kg·K), density 1,920 kg/m^3 [11]. There is a range of thermal properties for brick. The values cited here are in the middle of the range. The effects of varying the properties will be discussed in Section 6. Because of the long burn time of the Howard Street Tunnel fire, the simulations were carried out for as long as it was necessary to achieve a relatively constant wall surface temperature. Once all of the solid surfaces within the tunnel (tunnel wall, train car steel walls) heated up to steady-state, it was assumed that the gas temperature would also remain steady.

There is a fair amount of uncertainty as to how large a spill area was created following the rupture of the tank car carrying the tripropylene. It was reported by the NTSB that the tripropylene spilled from a 1.5 inch (4 cm) hole near the bottom of the cylindrical tank [1]. The initial flow from the hole was estimated via the relation

$$\dot{V} = C\,A\,\sqrt{\frac{2\,\Delta P}{\rho}} \tag{2}$$

where C is an orifice coefficient, equal to about 0.7, A is the area of the hole, ΔP is essentially the pressure near the bottom of tank, and ρ is the density of the liquid. From this relation, it was estimated that the fuel initially spilled at a rate of approximately 1,000 L/min (250 gal/min). The rate decreased over time as the pressure at the hole decreased, although it is possible that the heat from the fire could have slowed the rate at which the pressure decreased by heating up the air within the tank. In any event, we can conservatively bracket the time required for the car to empty its contents from two to four hours.

The heat of combustion of tripropylene is about 44,300 kW/kg; its density is 0.74 kg/L. If the spilling fuel were to have burned immediately upon its release without forming a pool, the heat release rate of the fire would have been about 1,000 MW. Rough calculations were performed initially that indicated that a fire of this size could not have been sustained in the tunnel due to the lack of sufficient oxygen to consume the fuel. Thus, it was assumed that the spilling tripropylene soaked into the roughly 1 ft (30 cm) layer of ballast (fist-sized rocks) between and below the ties of the railroad tracks.

Burning rates of liquid fuels are typically measured in deep obstruction-free pools. Because both the area and burning rate of the fuel-soaked ballast are subject to considerable uncertainty, a range of burn areas and rates had to be considered in the study. As a first estimate, the burn area was assumed to have been 12 m^2 (130 ft^2). The burn area was increased from this size to determine the sensitivity of the tunnel temperatures to the size of the pool. The car carrying the tripropylene held approximately 110,000 L (28,700 gal). The time required to burn this much fuel is proportional to the burn area. Based on measurements of similar liquid hydrocarbon fuels burning in deep pools under fully-ventilated conditions [10], the peak burning rate of the tripropylene (nonene) per unit area was estimated to have been 0.06 kg/(m^2·s) or 0.08 L/(m^2·s) (7 gal/(ft^2·h)). Although the tripropylene did not necessarily form a deep pool, the estimate was applied to the burning rate of fuel-soaked ballast. To simplify the analysis, rather than varying the area of the fuel bed and the burning rate per unit area, the burning rate was assumed constant and the area varied.

It is difficult to estimate how long the fire in the tunnel would have lasted for a number of reasons. First, some of the fuel could have drained through grates in the floor of the tunnel. Second, a considerable fraction of the fuel would have evaporated but not burned due to the high heat flux

to the fuel bed but low oxygen level in the tunnel. A tunnel fire is an example of a very inefficient combustion system. Unlike in an efficient commercial furnace, the large amount of fuel and small amount of oxygen lead to a substantial increase in the production of soot (black smoke), carbon monoxide, unburned fuel, and various other products of incomplete combustion.

Complicating the estimate of the burn time is the fact that at 6:19 pm, approximately three hours after the fire started, a water main crossing just below the tunnel ceiling and running perpendicular to the tunnel at Lombard Street, ruptured, and water poured into the tunnel. Estimates of the amount of water spilled vary, but it was substantial. It was observed by Baltimore City Fire Department (BCFD) officials that water filled the intersection of Howard and Lombard Streets to a depth of about 1 ft (30 cm). The water had a significant effect on the fire below because at 6:58 pm, 39 min after the pipe ruptured, BCFD officials commented that there was a noticeable change in the color of the smoke pouring from the Mount Royal portal, from dark black to gray. Preliminary calculations showed that the velocity of the smoke and hot gases near the ceiling of the tunnel flowing towards the Mount Royal portal was on the order of 1 m/s (3 ft/s, 2 mi/h). At this rate, it would have taken on the order of 30 min for the smoke to have traversed the 1,900 m (6,300 ft) between Lombard Street and Mount Royal. Because some time would have been required for the water to affect the fire, plus a weaker fire would not have driven the smoke as quickly, the appearance of whiter smoke approximately 40 min after the pipe rupture can be attributed directly to the introduction of a substantial amount of water into the tunnel near the fire.

It is not known to what extent the water reduced the size of the fire. NTSB interviews indicate that when fire fighters were able to approach the tripropylene car twelve hours after the fire started, it was not burning. It can thus be assumed that the fire burned at full strength for three hours, potentially burned for several more hours but at a reduced rate due to the introduction of water, and exhausted itself either due to a lack of fuel or extinguishment by water after twelve hours. Smoldering fires continued in the closed box cars for several days during which time emergency responders pulled the cars from the tunnel.

The calculations to be discussed next simulate the first half hour of the fire. The predicted gas and surface temperatures reach a steady-state in this amount of time, allowing for an assessment of the thermal environment for the time period before the water main break.

5 Calculation Results

Shown in Fig. 10 are vertical centerline temperature contours at two stages during the simulated fire in the Howard Street Tunnel. Initially, the fire would have been well-ventilated; that is, it would have had access to a supply of oxygen comparable to the outside. However, as the tunnel filled with smoke and other combustion products, the fire would have become oxygen-limited, especially on the up-slope side of the fire. Since the air movement in the tunnel would have been biased towards the uphill portal (Mount Royal Station), one would expect to see the fire pushed over towards the right in the figures. This effect was more pronounced in the Memorial Tunnel experiment, where the air flow through the tunnel was uni-directional uphill. The Howard Street Tunnel is about one-fourth as steep as the Memorial Tunnel, and smoke was observed pouring from both portals. The uphill side of the fire shows slightly lower oxygen concentrations, as seen in Fig. 11.

The segment of the tunnel shown is a small fraction of the overall length. The entire tunnel volume was included in the calculation so that the mixing of fresh air and hot smoke along the entire tunnel length could be simulated. The mixing process dictates where the boundary between the hot upper layer and cooler lower layer will be located. This is an important finding because train cars that were pulled from the tunnel a few days after the initial derailment show discoloration above a height of a few meters. The level at which the discoloration begins varies, depending on how far from the fire the car was. Photos of some tank cars show damage roughly two-thirds of the way up the height of the car, while some box cars show damage starting about one-third of the way up. See Figs. 13 – 15.

The extent of the damage to objects within the tunnel is a function of the gas temperature surrounding the object and the radiative heat flux to the object from nearby hot objects or fire. Typically, objects closer to the ground are subjected to less direct heating from hot gases, but they do absorb radiant energy from the hotter gas layer above. For the simulations of the Howard Street Tunnel fire, the temperature and heat flux was estimated at the tunnel ceiling and floor, to bracket the range of temperature and heat flux to which objects in the tunnel may have been exposed. The estimates indicate that surfaces that were exposed to direct flame impingement were subjected to heat fluxes in a range from 100 kW/m^2 to 150 kW/m^2. These surfaces would include the tunnel ceiling above the fire, and the sides of the rail cars directly within the fire. This magnitude of heat flux has been measured at Sandia National Laboratories in fire experiments involving large objects suspended in large, open hydrocarbon pool fires [12]. Surfaces that were exposed to the hot, smoke-laden gases flowing near the tunnel ceiling, like the tops of the rail cars, are estimated to have seen heat fluxes in the range of 40 kW/m^2 to 80 kW/m^2, depending on the proximity to the fire. Ultimately, the steel rail cars heated up to a temperature very near the gas temperature. After the tripropylene had been consumed, the closed rail cars containing smoldering paper products probably maintained a temperature on the order of 300 °C (570 °F), consistent with the temperature at which paper undergoes thermal degradation into pyrolyzates. The basis of this speculation is the fact that several cars burst into flames when they were opened up in the course of extinguishing the smoldering materials inside. The introduction of oxygen to the closed cars caused the transition from smoldering to flaming combustion.

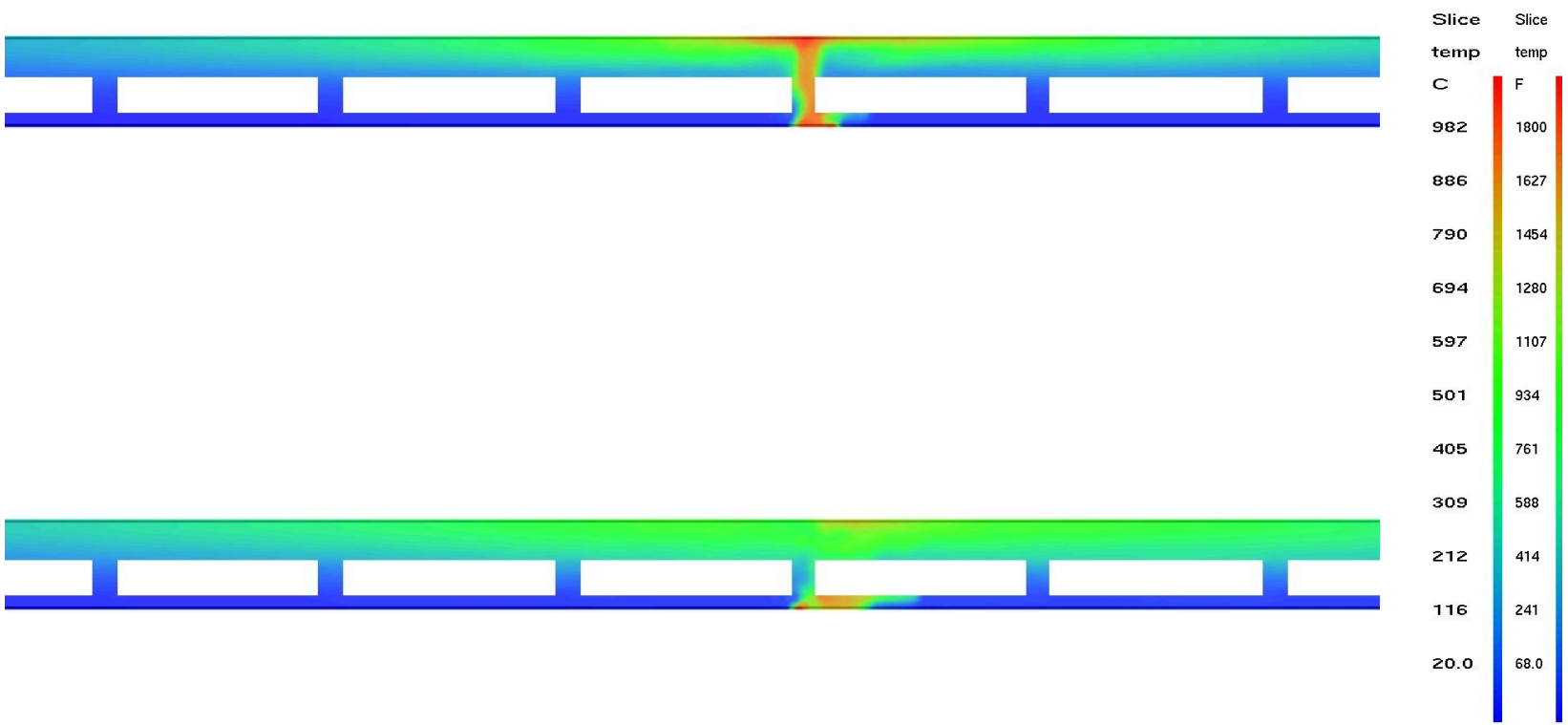

FIGURE 10: Predicted temperatures along the centerline vertical plane at 5 and 30 min after ignition of the Howard Street Tunnel fire. The region shown encompasses the rail cars nearest the tripropylene spill. The temperatures decrease in the tunnel as the fire becomes oxygen-limited. The white rectangular boxes in each frame represent rail cars through which the temperature slice cuts. The tunnel slopes upwards from left to right.

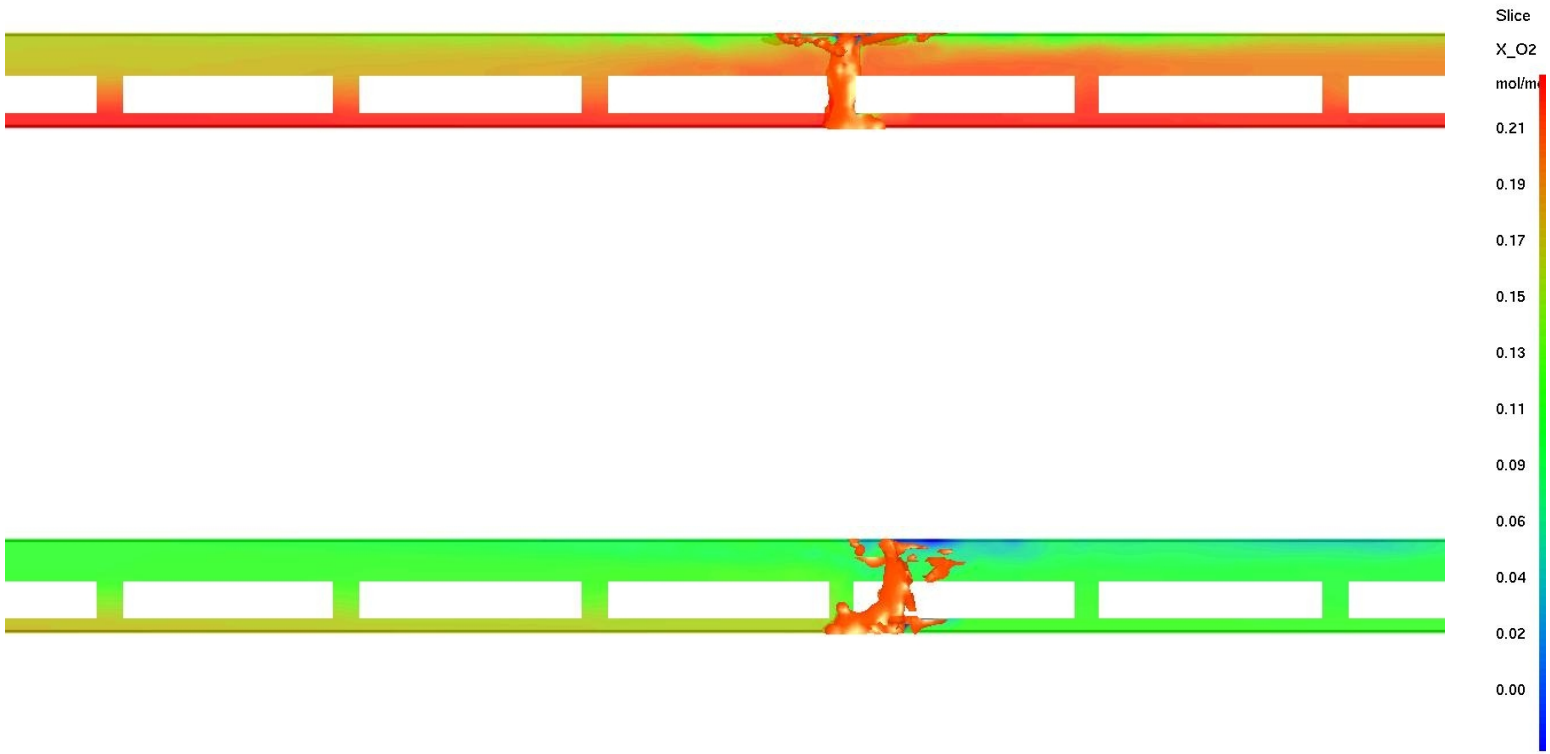

FIGURE 11: Predicted oxygen concentration along the centerline vertical plane at 5 and 30 min after ignition of the Howard Street Tunnel fire. The region shown encompasses the rail cars nearest the tripropylene spill. The flaming region is shown in orange. The white rectangular boxes in each frame represent the outline of the rail cars. The tunnel slopes upwards from left to right.

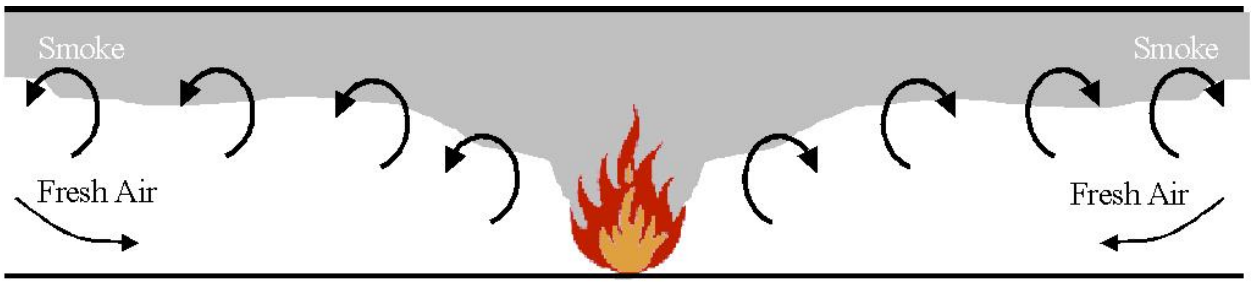

FIGURE 12: Schematic diagram showing how smoke and fresh air mix within a tunnel.

6 Analysis and Discussion

In this section, we will analyze the results of the calculations presented, and consider the uncertainty of the results by varying the most sensitive input parameters to the model. The first question to consider is how fast was the tripropylene consumed; next, what were the temperatures of the brick walls and steel rail cars; and finally, how would these findings change if the input parameters were varied. This is how most fire analysis is done – how much energy is produced, and where does this energy go?

6.1 Burning Rate

A fire requires fuel, oxygen and a source of heat to sustain itself. In a confined space, it is usually oxygen that is in short supply, thus the name given to these types of fires is "oxygen-limited." The size of the Howard Street Tunnel fire appears to have been limited to about 50 MW based on the various calculations that were performed.[3] In some calculations, only the pool area was specified, and the fuel was allowed to evaporate based on the thermal heat flux impinging on the fuel surface. In others, a fixed heat release rate was used based on the estimated size of the pool and the properties of the fuel. In both cases, the heat release rate was about 50 MW. Often more fuel vaporizes than is actually burned in oxygen-limited fires, and even the fuel that is consumed is not burned efficiently, hence the black smoke.

From the estimated heat release rate of the fire, we can estimate the amount of oxygen (and air) that reached the fire from outside the tunnel. Figure 12 is a schematic diagram showing how smoke and fresh air mix along the interface between the hot upper layer of smoke and cool lower layer of fresh air. Given that the tunnel is 2.65 km (1.65 mi) in length, much of the fresh air that entered the tunnel during the fire was mixed with the exiting smoke and never reached the fire. Given that most hydrocarbon fires (including tripropylene) consume oxygen at a rate of 13,000 kJ/kg, a 50,000 kW fire would consume oxygen at a rate of about 4 kg/s. The volume of air required to provide this amount of oxygen is about 14 m^3/s (30,000 cfm). Because most of the air reaching the fire would have had to come from the Camden and Mount Royal portals, the fire could not have burned fuel at a greater rate than it did because of oxygen limitations.

[3] To put this number in perspective, 50 MW (or 50,000 kW) is roughly the heat release rate of a small single family house engulfed in flames.

FIGURE 13: Box car from the Howard Street Tunnel. Photo courtesy of the National Transportation Safety Board.

FIGURE 14: Tripropylene tank car (#52) after the fire, shown from the left side. The fuel spilled out of hole near the bottom of the tank at the right. The car in front is a box car carrying paper (car #51 out of 60). Courtesy Nancy McAtee of the National Transportation Safety Board.

FIGURE 15: Right side of car #53, a tank car carrying hydrochloric acid. Courtesy Nancy McAtee of the National Transportation Safety Board.

6.2 Parameter Study

Throughout the course of the investigation into the thermal environment of the Howard Street Tunnel fire, several dozen simulations were performed based on descriptions of the train, the tunnel, and the fuel spill. An examination of photographs taken by the NTSB during and after the incident helped to narrow down the range of potential fire scenarios. The calculations showed small variations in results, but nothing that would significantly affect the overall conclusions.

The most important quantity in any fire analysis is the heat release rate of the fire. In fact, the focus of fire modeling is to predict how the energy from the fire is distributed throughout the volume of interest. As was discussed above, the fire in the Howard Street Tunnel was most likely oxygen-limited, that is, the heat release rate of the fire was constrained by the supply of oxygen, not fuel, which is usually the case with large fires in enclosures. In the calculations, the size of the pool of liquid fuel was varied, the parameters governing the evaporation process were varied, and various fixed fuel evaporation rates were prescribed. In all cases, the heat release rate of the fire was about 50 MW or less. The unburned fuel gases were mixed in with the exhaust gases and vented out the tunnel exits without having burned.

Given that the peak heat release rate of the fire was about 50 MW, the next issue to consider is how much of that energy was absorbed by the tunnel walls, and how much was lost to the atmosphere via the black smoke. Given the length of the tunnel, most of the fire's heat was absorbed by the walls. The temperature of the smoke exiting the tunnel at both ends was very nearly ambient, based on the results of the calculations. Since the tunnel walls were absorbing the heat, the thermal properties of the brick was an important consideration. Various sources in the heat transfer and fire literature [11, 13] report the thermal conductivity of brick to range between 0.5 W/(m·K) to 1.0 W/(m·K), the density 1,500 kg/m^3 to 3,000 kg/m^3, the specific heat 800 J/(kg·K) to 1000 J/(kg·K). Because the brick used in the Howard Street Tunnel is difficult to characterize, calculations were performed using a range of thermal properties for the brick walls to determine what effect this would have on the final temperatures within the tunnel. The baseline calculation was run with a thermal conductivity of 0.7 W/(m·K). Calculations with values of 0.45 W/(m·K) and 1.0 W/(m·K) were run to check the sensitivity of the results. The peak surface temperature at the ceiling for the baseline case was approximately 700 °C (1,300 °F), whereas when the lower value of the thermal conductivity was used, the peak temperature was approximately 800 °C (1,500 °F). When the higher value of conductivity was used, the peak temperature was approximately 600 °C (1,100 °F). It is expected that a more conductive wall lining would be less hot than a more insulating lining because the more conductive lining conducts heat away at a greater rate. Note that these temperatures are being rounded off to the nearest hundred degrees Celsius to indicate that the location of the hottest point on the tunnel ceiling shifts with the fire. These temperatures were predicted where flames were simulated to have impinged on the ceiling. The intent of this study is to gauge the sensitivity of the simulation results to the input parameters.

One additional sensitivity study was performed simply as a result of varying the geometry of the tunnel and train cars contained within the tunnel as more detailed information was made available. The original simulations of the fire were performed under the assumption that the tunnel was nominally 6.1 m (20 ft) high and 9.1 m (30 ft) wide. The cars were assumed to be solid blocks 3.0 m (10 ft) wide and 4.0 m (13 ft) high with 1.0 m (3 ft) of void space beneath to represent the undercarriage. Most of the cars were centered in the tunnel, but several of the derailed cars were offset based on the diagram of the accident scene provided by the NTSB. The cars in the simulation

served as targets of thermal radiation and obstructions limiting the airflow to the fire. Specific damage to the cars was not included in the simulations. Throughout the study, the car dimensions remained the same, but the tunnel dimensions were varied based on information provided by the NTSB. In the vicinity of the fire, the actual dimensions of the tunnel are 9.9 m (32.5 ft) wide by 6.4 m (21.0 ft) high. The section of the tunnel north of the accident is approximately 8.2 m (27 ft) wide by 6.7 m (22 ft) high. Because of resolution limits of the numerical grid, the width of 8.2 m (27 ft) and a height of 7.3 m (24 ft) was used for most of the simulations. It was found that the variations in tunnel width and height had no measurable effect on the results of the study.

7 Conclusion

The Howard Street Tunnel fire in Baltimore in July, 2001, has been modeled using the Fire Dynamics Simulator, a computational fluid dynamics fire model developed by the National Institute of Standards and Technology. The objective of the calculations has been to quantify the peak gas and surface temperatures that were likely reached during a several hour period in which a pool of spilled tripropylene burned. As a validation of the numerical model, several fire tests conducted in a decommissioned highway tunnel in West Virginia were simulated, with peak temperatures between experiment and model agreeing within about 50 °C (90 °F).

The simulations of the Howard Street Tunnel fire address the behavior of the fire from its ignition until the rupture of a water main three hours later. The simulations suggest that during this time period the fire was oxygen-limited, that is, the heat release rate of the fire was limited to about 50 MW by the amount of oxygen that could reach the fire. During this time, some of the spilled tripropylene evaporated but could not burn for lack of oxygen, and some drained off through grates in the tunnel floor. The exact distribution of the fuel is hard to predict, thus predicting the duration of the fire, with or without the rupturing of the water main, would be difficult. Between three and twelve hours after ignition, the tripropylene fire self-extinguished either due to a lack of fuel or suppression by water. Beyond twelve hours, the combustible products within the closed box cars continued to smolder for several days, but at temperatures far less than those experienced during the flaming combustion of the liquid fuel.

The peak calculated temperatures within the tunnel during the first three hours (before the water main rupture) were approximately 1,000 °C (1,800 °F) within the flaming regions or about half of the length of a rail car, and approximately 500 °C (900 °F) when averaged over a length of the tunnel equal to the length of three to four rail cars. Because of the insulation provided by the thick brick walls of the tunnel, the temperatures within a few car lengths of the fire were relatively uniform, consistent with what one would expect to find in an oven or furnace. According to the calculations, the peak calculated wall surface temperature reached about 800 °C (1,500 °F) where the flames were directly impinging, and 400 °C (750 °F) over the length of three to four rail cars. The steel temperature of the rail cars would be expected to be similar to the surrounding gas temperature because of the long exposure time and high thermal conductivity of steel.

A sensitivity study was undertaken to ensure that variations in the physical parameters of the model and the accident scenario would not lead to dramatic changes in the overall results. The fact that the fire within the tunnel would have very soon become oxygen-limited reduced the possibility for wide variations in the outcome of the study.

References

[1] NTSB Fire Group – Factual Report. NTSB Public Docket, Report Issue Date: October 2002. NTSB Case Reference Number: DCA 01 MR 004; Accident Site Location Reference: Baltimore, MD (Howard Street Tunnel); Accident Date Reference: July 18, 2001.

[2] K.B. McGrattan, H.R. Baum, R.G. Rehm, G.P. Forney, J.E. Floyd, and S. Hostikka. Fire Dynamics Simulator (Version 2), Technical Reference Guide. Technical Report NISTIR 6783, National Institute of Standards and Technology, Gaithersburg, Maryland, November 2001.

[3] K.B. McGrattan, G.P. Forney, J.E. Floyd, and S. Hostikka. Fire Dynamics Simulator (Version 2), User's Guide. Technical Report NISTIR 6784, National Institute of Standards and Technology, Gaithersburg, Maryland, November 2001.

[4] S. Hostikka, H.R. Baum, and K.B. McGrattan. Large Eddy Simulations of the Cone Calorimeter. In *Proceedings of US Section Meeting of the Combustion Institute, Oakland, California*, March 2001.

[5] K.B. McGrattan, H.R. Baum, and R.G. Rehm. Large Eddy Simulations of Smoke Movement. *Fire Safety Journal*, 30:161–178, 1998.

[6] K.B. McGrattan, A. Hamins, and D. Stroup. Sprinkler, Smoke & Heat Vent, Draft Curtain Interaction — Large Scale Experiments and Model Development. Technical Report NISTIR 6196-1, National Institute of Standards and Technology, Gaithersburg, Maryland, September 1998.

[7] International Collaborative Project to Evaluate Fire Models for Nuclear Power Plant Applications – Summary of Planning Meeting. Technical Report NUREG/CP-0170, Nuclear Regulatory Commission, 2000.

[8] Memorial Tunnel Fire Ventilation Test Program. Test Report, Massachusetts Highway Department, 1995.

[9] J. Quintiere. A Perspective on Compartment Fire Growth. *Combustion Science and Technology*, 39:11–54, 1984.

[10] V. Babrauskas. *SFPE Handbook*, chapter Burning Rates. National Fire Protection Association, Quincy, Massachusetts, 2nd edition, 1995.

[11] F.P. Incropera and D.P. De Witt. *Fundamentals of Heat and Mass Transfer*. John Wiley and Sons, New York, 3rd edition, 1990.

[12] M.A. Kramer, M. Greiner, and J.A. Koski. Radiation Heat Transfer to the Leeward Side of a Massive Object Suspended over a Pool Fire. In *Proceedings of 2001 ASME International Mechanical Engineering Congress and Exposition*. American Society of Mechanical Engineering, November 2001. IMECE2001/HTD-24250.

[13] J.G. Quintiere. *Principles of Fire Behavior*. Delmar Publishers, Albany, New York, 1998.

[14] R.G. Rehm and H.R. Baum. The Equations of Motion for Thermally Driven, Buoyant Flows. *Journal of Research of the NBS*, 83:297–308, 1978.

[15] H.R. Baum and K.B. McGrattan. Simulation of Large Industrial Outdoor Fires. In *Fire Safety Science – Proceedings of the Sixth International Symposium*. International Association for Fire Safety Science, 1999.

[16] C. Huggett. Estimation of the Rate of Heat Release by Means of Oxygen Consumption Measurements. *Fire and Materials*, 4:61–65, 1980.

[17] W. Grosshandler. RadCal: A Narrow Band Model for Radiation Calculations in a Combustion Environment. NIST Technical Note (TN 1402), National Institute of Standards and Technology, Gaithersburg, Maryland 20899, 1993.

[18] G.D. Raithby and E.H. Chui. A Finite-Volume Method for Predicting Radiant Heat Transfer in Enclosures with Participating Media. *Journal of Heat Transfer*, 112(2):415–423, 1990.

[19] J.P. Holman. *Heat Transfer*. McGraw-Hill, New York, 5th edition, 1989.

[20] K. Prasad, C. Li, K. Kailasanath, C. Ndubizu, R. Ananth, and P.A. Tatem. Numerical modelling of methanol liquid pool fires. *Combustion Theory and Modelling*, 3:743–768, 1999.

A Numerical Method

The Fire Dynamics Simulator (FDS) is publicly available software maintained by the National Institute of Standards and Technology (NIST). It can be downloaded from the web site

`http://fire.nist.gov/fds`

The numerical method used in FDS is documented in Reference [2], and instructions on how to use the model are given in Reference [3]. As of the publication of this report, the released version of FDS is 2.0. Some of the physical mechanisms discussed below needed for this project will be available in the next release of FDS.

A.1 Conservation Equations

An approximate form of the Navier-Stokes equations appropriate for low Mach number applications is used in the model. The approximation involves the filtering out of acoustic waves while allowing for large variations in temperature and density [14]. This gives the equations an elliptic character, consistent with low speed, thermal convective processes. To handle sub-grid scale convective motion, a large eddy simulation (LES) technique is used in which the large-scale eddies are computed directly and the sub-grid scale dissipative processes are modeled.

Consider the conservation equations of mass, momentum and energy for a thermally-expandable, multi-component mixture of ideal gases [14]:

Conservation of Mass

$$\frac{\partial \rho}{\partial t} + \nabla \cdot \rho \mathbf{u} = 0 \tag{3}$$

Conservation of Species

$$\frac{\partial}{\partial t}(\rho Y_l) + \nabla \cdot \rho Y_l \mathbf{u} = \nabla \cdot (\rho D)_l \nabla Y_l + \dot{W}_l''' \tag{4}$$

Conservation of Momentum

$$\rho \left(\frac{\partial \mathbf{u}}{\partial t} + (\mathbf{u} \cdot \nabla)\mathbf{u} \right) + \nabla p = \rho \mathbf{g} + \nabla \cdot \tau \tag{5}$$

Conservation of Energy

$$\frac{\partial}{\partial t}(\rho h) + \nabla \cdot \rho h \mathbf{u} - \frac{Dp}{Dt} = \dot{q}''' - \nabla \cdot \mathbf{q}_r + \nabla \cdot k \nabla T + \nabla \cdot \sum_l h_l (\rho D)_l \nabla Y_l \tag{6}$$

The symbols have their usual meanings: ρ is the density, $\mathbf{u}$ is the velocity vector, Y_l is the mass fraction of species l, $\dot{W}_l'''$ is the mass production rate of species l per unit volume, p is the pressure, $\mathbf{g}$ is the gravity vector, τ is the viscous stress tensor, h is the enthalpy, $\dot{q}'''$ is the heat release rate per unit volume, $\mathbf{q}_r$ is the radiative flux, T is the temperature, k is the thermal conductivity, and D is the material diffusivity. The energy driving the system is represented by the heat release rate $\dot{q}'''$ in Eq. (6). The term $Dp/Dt = \partial p/\partial t + \mathbf{u} \cdot \nabla p$ is a material derivative.

The conservation equations are supplemented by an equation of state relating the thermodynamic quantities density, pressure and enthalpy; ρ, p and h. The pressure is decomposed into three components

$$p = p_0 - \rho_\infty g z + \tilde{p} \tag{7}$$

The first term on the right hand side is the "background" pressure, the second is the hydrostatic contribution, and the third is the flow-induced perturbation pressure. For most applications, p_0 is constant. However, if the enclosure is tightly sealed, p_0 is allowed to increase (or decrease) with time as the pressure within the enclosure rises due to thermal expansion or falls due to forced ventilation. Also, if the height of the domain is on the order of a kilometer, p_0 can no longer be assumed constant and must be considered a function of the altitude [15].

The purpose of decomposing the pressure is that for low-Mach number flows, it can be assumed that the temperature and density are inversely proportional, and thus the equation of state can be approximated [14]

$$p_0 = \rho T \mathcal{R} \sum (Y_i / M_i) = \rho T \mathcal{R} / M \tag{8}$$

The pressure p in the state and energy equations is replaced by the background pressure p_0 to filter out sound waves that travel at speeds that are much faster than typical flow speeds expected in fire applications. The low Mach number assumption serves two purposes. First, the filtering of acoustic waves means that the time step in the numerical algorithm is bound only by the flow speed as opposed to the speed of sound, and second, the modified state equation leads to a reduction in the number of dependent variables in the system of equations by one. The energy equation (6) is never explicitly solved, but its source terms are included in the expression for the flow divergence, an important quantity in the analysis to follow.

A.2 Combustion

The mixture fraction combustion model is based on the assumption that large-scale convective and radiative transport phenomena can be simulated directly, but physical processes occurring at small length and time scales must be represented in an approximate manner. The nature of the approximations employed are necessarily a function of the spatial and temporal resolution limits of the computation, as well as our current (often limited) understanding of the phenomena involved.

The actual chemical rate processes that control the combustion energy release are often unknown in fire scenarios. Even if they were known, the spatial and temporal resolution limits imposed by both present and foreseeable computer resources places a detailed description of combustion processes beyond reach. Thus, the model adopted here is based on the assumption that the combustion is mixing-controlled. This implies that all species of interest can be described in terms of a mixture fraction $Z(\mathbf{x},t)$. The mixture fraction is a conserved quantity representing the fraction of material at a given point that originated as fuel. The relations between the mass fraction of each species and the mixture fraction are known as "state relations". The state relation for the oxygen mass fraction provides the information needed to calculate the local oxygen mass consumption rate. The form of the state relation that emerges from classical laminar diffusion flame theory is a piecewise linear function. This leads to a "flame sheet" model, where the flame is a two dimensional surface embedded in a three dimensional space. The local heat release rate is computed from the local oxygen consumption rate at the flame surface, assuming that the heat release rate

is directly proportional to the oxygen consumption rate, independent of the fuel involved. This relation, originally proposed by Huggett [16], is the basis of oxygen calorimetry.

Start with the most general form of the combustion reaction

$$\nu_F \text{ Fuel} + \nu_O \text{ O}_2 \rightarrow \sum_i \nu_{P,i} \text{ Products} \tag{9}$$

The numbers ν_i are the stoichiometric coefficients for the overall combustion process that reacts fuel "F" with oxygen "O" to produce a number of products "P". The stoichiometric equation (9) implies that the mass consumption rates for fuel and oxidizer are related as follows:

$$\frac{\dot{m}'''_F}{\nu_F M_F} = \frac{\dot{m}'''_O}{\nu_O M_O} \tag{10}$$

The mixture fraction Z is defined as:

$$Z = \frac{sY_F - \left(Y_O - Y_O^\infty\right)}{sY_F^I + Y_O^\infty} \quad ; \quad s = \frac{\nu_O M_O}{\nu_F M_F} \tag{11}$$

By design, it varies from $Z = 1$ in a region containing only fuel to $Z = 0$ where the oxygen mass fraction takes on its undepleted ambient value, Y_O^∞. Note that Y_F^I is the fraction of fuel in the fuel stream. The quantities M_F and M_O are the fuel and oxygen relative molecular masses, respectively. The mixture fraction satisfies the conservation law

$$\rho \frac{DZ}{Dt} = \nabla \cdot \rho D \nabla Z \tag{12}$$

obtained from a linear combination of the fuel and oxygen conservation equations. The assumption that the chemistry is "fast" means that the reactions that consume fuel and oxidizer occur so rapidly that the fuel and oxidizer cannot co-exist. The requirement that fuel and oxidizer simultaneously vanish defines a flame surface as:

$$Z(\mathbf{x},t) = Z_f \quad ; \quad Z_f = \frac{Y_O^\infty}{sY_F^I + Y_O^\infty} \tag{13}$$

The assumption that fuel and oxidizer cannot co-exist leads to the "state relation" between the oxygen mass fraction Y_O and Z

$$Y_O(Z) = \begin{cases} Y_O^\infty(1 - Z/Z_f) & Z < Z_f \\ 0 & Z > Z_f \end{cases} \tag{14}$$

State relations for both reactants and products can be derived by considering the following ideal reaction of a hydrocarbon fuel:

$$\begin{aligned} \text{C}_\text{x}\text{H}_\text{y} + \eta(\text{x} + \text{y}/4)\,(\text{O}_2 + 3.76\,\text{N}_2) \quad &\rightarrow \quad \max(0, 1-\eta)\,\text{C}_\text{x}\text{H}_\text{y} + \min(1,\eta)\,\text{x}\,\text{CO}_2 + \\ \min(1,\eta)\,(\text{y}/2)\,\text{H}_2\text{O} \quad &+ \quad \max(0,\eta-1)\,(\text{x}+\text{y}/4)\,\text{O}_2 + \eta(\text{x}+\text{y}/4)3.76\,\text{N}_2 \end{aligned} \tag{15}$$

Here η is a parameter ranging from 0 (all fuel with no oxygen) to infinity (all oxygen with no fuel). A correspondence between η and Z is obtained by applying the definition of Z (Eq. 11) to the left hand side of Eq. (15). Mass fractions of the products of the infinitely fast reaction (including

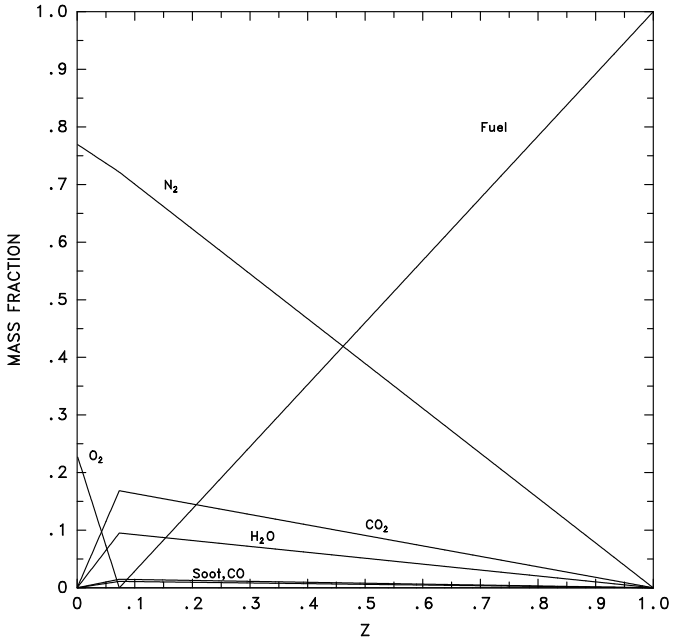

FIGURE 16: State relations for nonene. The soot yield is assumed to be 0.15 and the CO yield is assumed to be 0.20, where the yield is the mass of product produced per mass of fuel burned.

excess fuel or oxygen) can be obtained from the right hand side of Eq. (15). State relations for the ideal reaction of nonene and air is shown in Fig. 16.

An expression for the local heat release rate can be derived from the conservation equations and the state relation for oxygen. The starting point is Huggett's [16] relationship for the heat release rate as a function of the oxygen consumption

$$\dot{q}''' = \Delta H_O \dot{m}_O''' \tag{16}$$

Here, ΔH_O is the heat release rate per unit mass of oxygen consumed. The oxygen mass conservation equation

$$\rho \frac{DY_O}{Dt} = \nabla \cdot \rho D \nabla Y_O + \dot{m}_O''' \tag{17}$$

can be transformed into an expression for the local heat release rate using the conservation equation for the mixture fraction (12) and the state relation for oxygen $Y_O(Z)$.

$$-\dot{m}_O''' = \nabla \cdot \left(\rho D \frac{dY_O}{dZ} \nabla Z \right) - \frac{dY_O}{dZ} \nabla \cdot \rho D \nabla Z = \rho D \, \frac{d^2 Y_O}{dZ^2} |\nabla Z|^2 \tag{18}$$

Neither of these expressions for the local oxygen consumption rate is particularly convenient to apply numerically because of the discontinuity of the derivative of $Y_O(Z)$ at $Z = Z_f$. However, an expression for the oxygen consumption rate per unit area of flame sheet can be derived from Eq. (18)

$$-\dot{m}_O'' = \left. \frac{dY_O}{dZ} \right|_{Z<Z_f} \rho D \, \nabla Z \cdot \mathbf{n} \tag{19}$$

In the numerical algorithm, the local heat release rate is computed by first locating the flame sheet, then computing the local heat release rate per unit area, and finally distributing this energy to the grid cells cut by the flame sheet. In this way, the ideal, infinitely thin flame sheet is smeared out over the width of a grid cell, consistent with all other gas phase quantities.

A.3 Thermal Radiation

The Radiative Transport Equation (RTE) for a non-scattering gas is

$$\mathbf{s}\cdot\nabla I_\lambda(\mathbf{x},\mathbf{s}) = \kappa(\mathbf{x},\lambda)\ [I_b(\mathbf{x}) - I(\mathbf{x},\mathbf{s})] \tag{20}$$

where $I_\lambda(\mathbf{x},\mathbf{s})$ is the radiation intensity at wavelength λ, $I_b(\mathbf{x})$ is the source term given by the Planck function, $\mathbf{s}$ is the unit normal direction vector and $\kappa(\mathbf{x})$ is the absorption coefficient. The source term can be written as a fraction of the blackbody radiation

$$I_b = \sigma\, T^4/\pi \tag{21}$$

where σ is the Stefan-Boltzmann constant. In most large-scale fire scenarios soot is the most important combustion product controlling the thermal radiation from the fire and hot smoke. As the radiation spectrum of soot is continuous, it is possible to assume that the gas behaves as a gray medium. The spectral dependence is lumped into one absorption coefficient. For the calculation of the gray gas absorption coefficient, κ, a narrow-band model, RADCAL [17], has been implemented in FDS. At the start of a simulation the absorption coefficient is tabulated as a function of mixture fraction and temperature. During the simulation the local absorption coefficient is found by table-lookup.

The boundary condition for the radiation intensity leaving a gray diffuse wall is given as

$$I_w(\mathbf{s}) = \varepsilon I_{bw} + \frac{1-\varepsilon}{\pi}\int_{\mathbf{s}'\cdot\mathbf{n}_w<0} I_w(\mathbf{s}')\ |\mathbf{s}'\cdot\mathbf{n}_w|\ d\Omega \tag{22}$$

where $I_w(\mathbf{s})$ is the intensity at the wall, ε is the emissivity, and I_{bw} is the black body intensity at the wall.

The radiative transport equation (20) is solved using techniques similar to those for convective transport in finite volume methods for fluid flow [18], thus the name given to it is the Finite Volume Method (FVM). To obtain the discretized form of the RTE, the unit sphere is divided into a finite number of solid angles. In each grid cell a discretized equation is derived by integrating equation (20) over the cell ijk and the control angle $\delta\Omega^l$, to obtain

$$\int_{\Omega^l}\int_{V_{ijk}} \mathbf{s}\cdot\nabla I_n(\mathbf{x},\mathbf{s})\,dV\,d\Omega = \int_{\Omega^l}\int_{V_{ijk}} \kappa_n(\mathbf{x})\ \left[I_{b,n}(\mathbf{x}) - I_n(\mathbf{x},\mathbf{s})\right] dV\,d\Omega \tag{23}$$

The volume integral on the left hand side is replaced by a surface integral over the cell faces using the divergence theorem. Assuming that the radiation intensity $I(\mathbf{x},\mathbf{s})$ is constant on each of the cell faces, the surface integral can be approximated by a sum over the cell faces.

The radiant heat flux vector $\mathbf{q}_r$ is defined

$$\mathbf{q}_r(\mathbf{x}) = \int \mathbf{s} I(\mathbf{x},\mathbf{s})\ d\Omega \tag{24}$$

The radiative loss term in the energy equation is

$$-\nabla\cdot\mathbf{q}_r(\mathbf{x}) = \kappa(\mathbf{x})\,[U(\mathbf{x}) - 4\pi I_b(\mathbf{x})] \quad ; \quad U(\mathbf{x}) = \int_{4\pi} I(\mathbf{x},\mathbf{s})\,d\Omega \tag{25}$$

In words, the net radiant energy gained by a grid cell is the difference between that which is absorbed and that which is emitted.

A.4 Convective Heat Transfer to Walls

The heat flux to a solid surface consists of gains and losses from convection and radiation. The radiative flux at the surface is obtained from the boundary condition for the radiation equation, Eq. (22).

The convective heat flux to the surface is obtained from a combination of natural and forced convection correlations

$$\dot{q}_c'' = h\,\Delta T \quad \text{W/m}^2 \quad ; \quad h = \max\left[C\,|\Delta T|^{\frac{1}{3}} \quad , \quad \frac{k}{L}\,0.037\,\text{Re}^{\frac{4}{5}}\,\text{Pr}^{\frac{1}{3}}\right] \quad \text{W/(m}^2\cdot\text{K)} \tag{26}$$

where ΔT is the difference between the wall and the gas temperature (taken at the center of the grid cell abutting the wall), C is the coefficient for natural convection (1.43 for a horizontal surface and 0.95 for a vertical surface) [19], L is a characteristic length related to the size of the physical obstruction, k is the thermal conductivity of the gas, and the Reynolds Re and Prandtl Pr numbers are based on the gas flowing past the obstruction. Since the Reynolds number is proportional to the characteristic length, L, the heat transfer coefficient is weakly related to L. For this reason, L is taken to be 1 m for most calculations.

If the surface material is assumed to be thermally-thick, a one-dimensional heat conduction equation for the material temperature, $T_s(x,t)$, is applied in the direction x pointing into the air/solid interface ($x = 0$)

$$\rho_s\,c_s\,\frac{\partial T_s}{\partial t} = k_s\,\frac{\partial^2 T_s}{\partial x^2} \quad ; \quad -k_s\frac{\partial T_s}{\partial x}(0,t) = \dot{q}_c'' + \dot{q}_r'' - \dot{m}''\,\Delta H_v \tag{27}$$

where ρ_s, c_s and k_s are the (constant) density, specific heat and conductivity of the material; $\dot{q}_c''$ is the convective and $\dot{q}_r''$ is the (net) radiative heat flux at the surface, $\dot{m}''$ is the mass loss rate if burning is occurring, and ΔH_v is the heat of vaporization. It is assumed that fuel pyrolysis takes place at the surface; thus the heat required to vaporize fuel is extracted from the incoming energy flux.

The rate at which liquid fuel evaporates when burning is a function of the liquid temperature and the concentration of fuel vapor above the pool surface. Equilibrium is reached when the partial pressure of the fuel vapor above the surface equals the Clausius-Clapeyron pressure

$$p_{cc} = p_0\,\exp\left[-\frac{h_v M_f}{\mathcal{R}}\left(\frac{1}{T_s} - \frac{1}{T_b}\right)\right] \tag{28}$$

where h_v is the heat of vaporization, M_f is the relative molecular mass, T_s is the surface temperature, and T_b is the boiling temperature of the fuel [20].

For simplicity, the liquid fuel itself is treated like a thermally-thick solid for the purpose of computing the heat conduction. There is no computation of the convection of the liquid within the pool.

CNWRA 2003-04
Revision 1

ANALYSIS OF RAIL CAR COMPONENTS EXPOSED TO A TUNNEL FIRE ENVIRONMENT

Prepared for

U.S. Nuclear Regulatory Commission
Contract NRC–02–02–012

Center for Nuclear Waste Regulatory Analyses
San Antonio, Texas

CNWRA 2003-04
Revision 1

ANALYSIS OF RAIL CAR COMPONENTS EXPOSED TO A TUNNEL FIRE ENVIRONMENT

Prepared for

U.S. Nuclear Regulatory Commission
Contract NRC–02–02–012

Prepared by

Andre S. Garabedian
Darrell S. Dunn
Asadul H. Chowdhury

Center for Nuclear Waste Regulatory Analyses
San Antonio, Texas

November 2002

ABSTRACT

Rail car components recovered from the train involved in the July 18, 2001, Howard Street Tunnel, Baltimore, Maryland train derailment and fire were used to estimate the fire duration and temperatures achieved by the components. Steel samples including sections of the box car panels and a bolt from an air brake assembly were analyzed using standard metallurgical methods to determine oxide layer thickness and the amount of metal lost as a result of the elevated temperature exposure. Aluminum alloy air brake valve assemblies, which melted as a consequence of the fire, were analyzed using a heat transfer model.

Analyses of the recovered components suggest the surface temperature of the steel reached 700 to 850 °C [1,292 to 1,562 °F] assuming an exposure time of 4 hours at the elevated temperatures. Independent assessment of fire duration could not be obtained from the steel components because the oxide scale thickness and metal loss are dependent on both time and temperature. Several limitations to the assessment of temperature were noted including the effects of oxide-scale spalling and post-fire atmospheric exposure for a period of more than 1 year.

Thermal analysis of the aluminum air brake valve body located approximately 10 m [33 ft] from the fire (at the brake end of Car 52) indicated melting occurred early in the fire event, and the temperature achieved by this component was at least 600 °C [1,112 °F]. A similar aluminum cover located at approximately 20 m [66 ft] from the fire (at the mid-point of Car 51) was only partially melted indicating its temperature may have reached 600 °C [1,112 °F] for a limited time, where an aluminum cover located approximately 30 m [98 ft] away from the spill site (at the brake end of Car 53) was not affected by the fire exposure at all. This temperature profile indicating a decrease in exposure temperature with distance away from the spill site was further substantiated by the lack of damage to other components, such as railcar exterior paint.

The analyses conducted suggest the temperatures achieved by materials present in a confined space fire are strongly dependent on the proximity of the component of interest to the fire source. Gas temperatures near the fire source were likely in excess of 800 °C [1,472 °F] for more than 30 minutes and the reaction of components in this region were likely influenced by the direct radiation from the fire. At a distance of approximately 20 m [66 ft] from the fuel source, where the dominant mode of heat transfer was convection, the exposure was capable of generating surface temperatures as high as 600 °C [1,112 °F], however, only for a much shorter duration.

CONTENTS

Section Page

ABSTRACT iii
FIGURES vii
ACKNOWLEDGMENTS ix

1 BACKGROUND 1-1

2 OBJECTIVES AND SCOPE OF WORK 2-1

3 SAMPLES COLLECTED TO DATE 3-1

3.1 Valve Assembly 3-1
3.2 Valve Materials 3-4
3.3 Steel Samples 3-4
3.4 Sand Samples 3-4

4 METALLURGICAL ANALYSES 4-1

4.1 Analysis Method 4-1
4.2 Results 4-3
4.3 Discussion 4-11

5 ALUMINUM SAMPLE THERMAL MODEL 5-1

5.1 Assumptions 5-1
5.2 Basic Equations 5-2
5.3 Analysis Method 5-3
5.4 Results 5-3
5.4.1 Ramp-Plateau Function 5-3
5.4.2 Ramp-Plateau-Decay Function 5-5
5.5 Discussion 5-6

6 CONCLUSIONS 6-1

7 REFERENCES 7-1

FIGURES

Figure		Page
3-1	The ABDX-L Control Valve	3-2
3-2	ABDX-L Service Portion Outline and Photograph	3-3
4-1	Oxidation Rate Constants for Fe-2¼Cr-1Mo Steel as a Function of Temperature	4-2
4-2	Reduction in Metal Thickness as a Function of Time for Isothermal Exposures in the Range of 827 to 1,177 °C [1,520 to 2,150 °F]	4-2
4-3	Metal Oxide Thickness as a Function of Time for Isothermal Exposures at Temperatures Ranging from 527 to 827 °C [980 to 1,520 °F]	4-3
4-4	Raman Spectra for Scales Recovered from Car 51	4-4
4-5	X-Ray Diffraction of Orange Colored Scales from Car 51	4-5
4-6	X-Ray Diffraction of Black Colored Oxide Scales from Car 51	4-5
4-7	Cross Section of Car 50 Roof Approximately 40 cm [16 in] from the Opposite End of the Roof Panel Section	4-6
4-8	Cross Section of Car 50 Roof Approximately 3 cm [1.2 in] from the Edge Directly Exposed to the Fire	4-7
4-9	Cross Section of Car 50 Roof at Edge Directly Exposed to the Fire	4-7
4-10	(a) Secondary Electron Image from Car 50 Roof at Edge Directly Exposed to the Fire, (b) Iron Image Map, (c) Oxygen Image Map	4-8
4-11	Scanning Electron Microscope Secondary Electron Image of Car 52 Air Brake Valve Bolt Showing Metal and Oxide Layer	4-9
4-12	Scanning Electron Microscope Secondary Electron Image of Car 52 Air Brake Valve Bolt Head Showing Iron and Aluminum and (b) Close-Up of Iron with Aluminum	4-10
5-1	ASTM E 1529 (1993) Ramp Function and Corresponding Aluminum Thermal Profile	5-4
5-2	Published Flame Temperature Ramp Function and Corresponding Aluminum Thermal Profile	5-4
5-3	Ramp-Plateau Function Demonstrates Melting at Published Flame Temperature for Exposure Times Greater than 360 Seconds	5-5
5-4	Ramp-Plateau-Decay Function and Corresponding Aluminum Thermal Profile	5-6
6-1	Air Brake Valve Found 20 + m [66 + ft] from Fuel Spill Site	6-1

ACKNOWLEDGMENTS

This report was prepared to document work performed by the Center for Nuclear Waste Regulatory Analyses (CNWRA) for the U.S. Nuclear Regulatory Commission (NRC) under Contract No. NRC–02–02–012. The activities reported here were performed on behalf of the NRC Office of Nuclear Material Safety and Safeguards, Spent Fuel Project Office. The report is an independent product of the CNWRA and does not necessarily reflect the views or regulatory position of the NRC.

The authors thank Yi-Ming Pan and Jason Huczek at Southwest Research Institute® for their technical assistance provided at various stages of the project. The authors thank Yi-Ming Pan, Jason Huczek, and B. Sagar for their technical and programmatic reviews of this report and C. Cudd and A. Woods for editorial reviews. The authors are thankful to C. Patton for assisting with the word processing and preparation of the report.

QUALITY OF DATA, ANALYSES, AND CODE DEVELOPMENT

DATA: No CNWRA-generated original data are contained in this report. Sources for other data should be consulted for determining the level of quality for those data.

ANALYSES AND CODES: Spreadsheet calculations were accomplished using Microsoft® Excel 2000. Analyses are documented in Scientific Notebook 550.

1 BACKGROUND

On July 18, 2001, a 60-car train, carrying flammable liquids, corrosive acids, paper products, and other commodities derailed while passing through the Howard Street Tunnel in Baltimore, Maryland. This incident derailed 11 cars, Cars 46 through 56, while on an upward slope of approximately 0.8 percent.

The derailment caused structural damage to Car 52, carrying approximately 106,000 L [28,000 gal] tripropylene, puncturing the base of the tank and initiating a fuel spill. A fire ensued, which burned freely for 3 hours. After approximately 3 hours into the event, a water main ruptured above the tunnel, introducing cooling water to the tunnel.

On August 27, 2002, the U.S. Nuclear Regulatory Commission (NRC) directed the Center for Nuclear Waste Regulatory Analyses to support the NRC and the National Transportation Safety Board in Washington, DC, to review and analyze the information obtained from the site visit of the stored, fire damaged cars from the Baltimore tunnel accident. Information obtained from the site visit and specimens from the rail cars were analyzed to estimate the duration of exposure and temperatures achieved by the fire-damaged cars. The objectives and scope of work discussed in this report are based on this directive.

2 OBJECTIVES AND SCOPE OF WORK

The goal of the project was to compile forensic evidence about the materials damaged during the tunnel fire and to use engineering methods to gain insight into the thermal environment the materials experienced during the fire. An estimation of the thermal environment at approximately 20 m [66 ft] on each side of the fire source will also be provided.

The thermal environment is defined by a temperature-time history. Two analyses needed to be conducted to establish this history:

Establish a Rough Temperature Achieved by Samples—Determine the rough-temperature profile by analyzing the phase change in materials collected from the site. These data will indicate the maximum temperatures achieved and may give a rough estimation of the duration. The source of such data is the metallurgical analysis of the exposed steel and aluminum components in the vicinity of the fire.

Predict the Duration—Correlate the rough-temperature history gained by metallurgical analysis to physical observations (e.g., melting). Using heat transfer equations and the metallurgical estimation of temperature, the predicted thermal environment can be imposed on the sample to determine whether damage, consistent with the damage observed, could have been caused by the exposure. In this case, the predictor will be the total phase change (melting) of a die-cast aluminum cover plate.

The analysis will focus on the vicinity of the tripropylene car before the water introduction because the thermal environment conditions are assumed to have been the worst. Analyses of the fire environment were directed, specifically, to the fire environment surrounding three air brake valve assemblies in the vicinity of the spilled tripropylene.

The prediction of the thermal environment in the vicinity of the air brake valve served to provide a better estimate for the thermal environment in the zones of interest {15–20 m [49.21–65.62 ft] to either side of a presumed spill site}. Data in the vicinity of the air brake valves will be extrapolated to other zones of interest, because there was no readily observable evidence of the thermal environment in these areas (e.g., no distinct melting, charring, or obvious deformation).

3 SAMPLES COLLECTED TO DATE

Several samples were collected from the site. Samples were chosen because of their proximity to the fire source and their level of damage.

These materials included

Steel Scale, Taken from the Brake End of Car 51—This location was adjacent to the brake end of Car 52 and was approximately 10–12 m [32.81–39.37 ft] uphill from the fire source.

Section of Roof Plate from Car 50—The steel section was taken from the roof of Car 50 because this location was the source of a substantial, secondary fire as a result of the prolonged paper fire.

Remainder of ABDX-L Air Brake Valve from Car 52—This air brake valve exhibited evidence of prolonged fire exposure. The valve includes several die-cast aluminum covers, which had completely melted as a result of the fire. The valve was found approximately 10 m [33 ft] uphill from the spill site, and approximately 1 m [3.3 ft] from the tunnel floor. A similar valve assembly was found at the midpoint of Car 51, approximately 20 m [66 ft] uphill from the fire source. Although the exact model type was not determined, the valve cover was clearly from the same family of products and was composed of the same aluminum alloy. A third air brake valve was found approximately 30 m [100 ft] from the spill site, and analyzed.

Exposed Bolts Remaining on Air Brake Valve Assembly—The bolts used to hold the die-cast aluminum covers were retrieved for subsequent analysis.

Sand Sample Adhered to the Base of Rail #44—Rail #44 (as identified by National Transportation Safety Board) was in the vicinity of the derailment and the fire source. The sand sample was taken from the south face of the track. The sand was of interest because it had exhibited some form of phase change, which transformed it from a powder to a consolidated mass.

New ABDX-L Air Brake Valve Cover and Attaching Bolts—A new valve cover and mounting hardware were provided by the manufacturer, WABTEC. These components were collected with the intent of defining a baseline for subsequent metallurgical analyses. Neither the aluminum cover nor the bolts were fully analyzed as part of this project because these samples were not received in time to be included in this report.

3.1 Valve Assembly

The valve assembly found on Car 52 was identified as an ABDX-L valve. The valve assembly located on Car 51 was also assumed to be an ABD valve assembly. A complete ABDX-L valve assembly is shown in Figure 3-1.

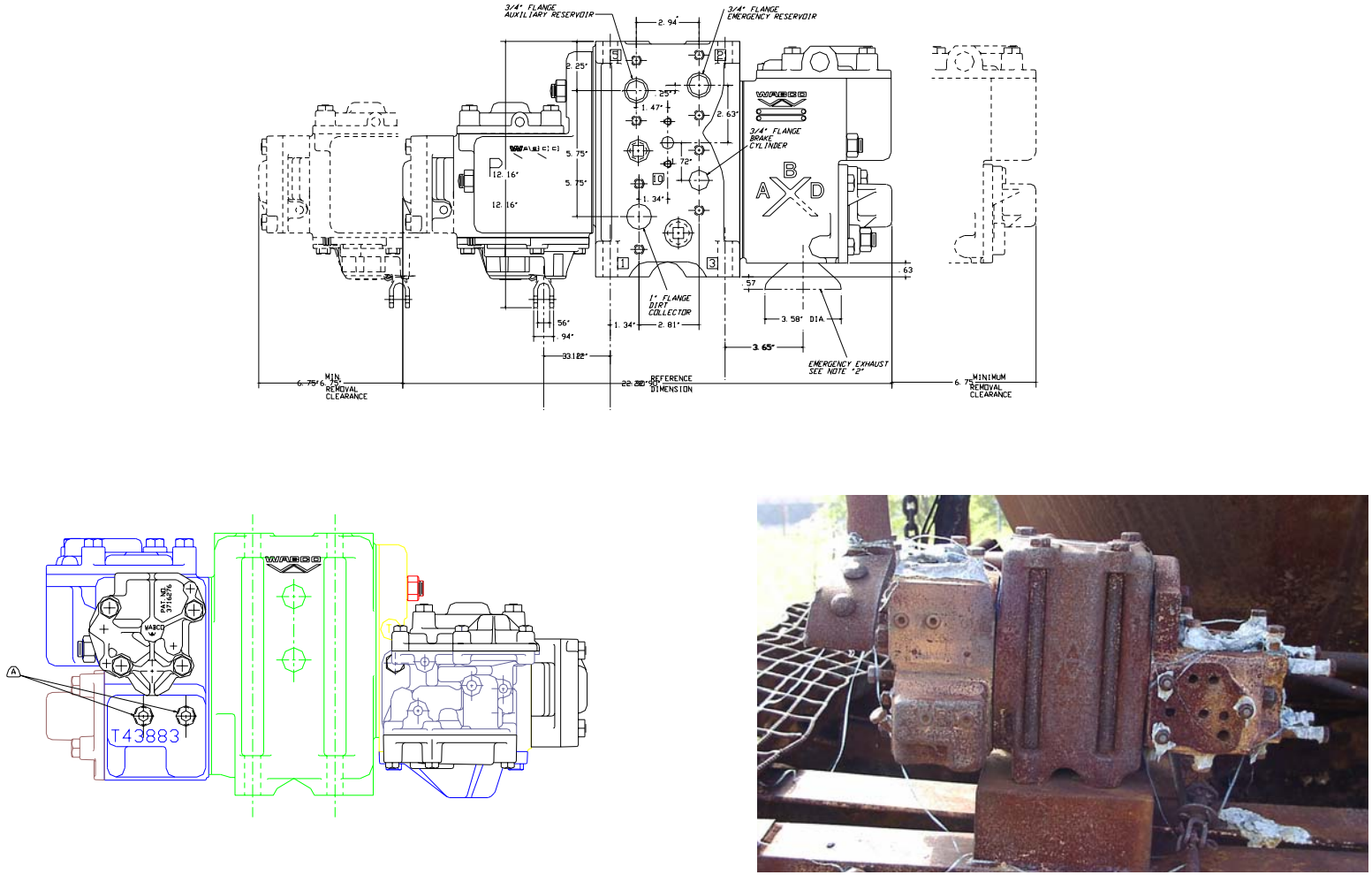

Figure 3-1. The ABDX-L Control Valve (Clockwise from Top: Valve Body Schematic, Photograph of Damaged Valve on Car 52, Corresponding Outline of the Valve Body)

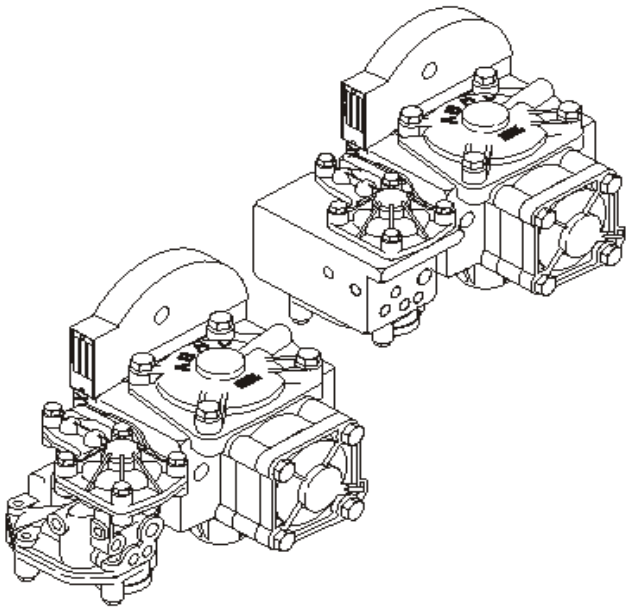

Figure 3-2. ABDX-L Service Portion Outline and Photograph

The standard ABDX-L-style valve consists of a normal service valve and an emergency valve. For this analysis, the damage observed on the service portion of the valve was analyzed (see Figure 3-2).

The primary area of interest in the analysis was the aluminum alloy cover over the release valve in the service portion of the valve assembly shown in Figure 3-2. The location of the cover is marked by the four bolts remaining on one side of the valve, and the associated aluminum residue.

The following assumptions were made regarding the aluminum component based on observations made during the site visit and photographic documentation of the rail cars after the accident:

Material:	Die-Cast Aluminum Alloy (ASTM B 85-99 Grade 360, aluminum-silicon alloy)
Dimensions[1]*:*	127 mm [5 in] diameter, 25.4 mm [1 in] thick
Heat Transfer Area:	Circumference and one side 228 cm² [35 in²]
Volume:	Assuming full depth of 322 cm³ [20 in³]
Orientation:	Vertical

3.2 Valve Materials

As stated by the manufacturer, the aluminum cover plate is composed of ASTM B 85-99 Alloy 360. It is assumed that the alloy is an aluminum-silicon alloy, the properties for which are common for a range of alloy percentages. The alloy has the following properties (Holman, 1990):

Thermal Conductivity (k):	177 W/m K
Density (ρ):	2,707 kg/m³
Specific Heat:	0.892 kJ/kg K
Melting Temperature:	600 ˚C [873 K]

3.3 Steel Samples

Samples were taken from Car 51 (scale), the air brake valve of Car 52 (bolt shown in Figure 3-2) and the roof of Car 50. Samples from the roof panel of Car 50 and the bolt from the airbrake valve of Car 52 were cut from their respective pieces using a low-speed saw. Care was taken not to disturb or heat the oxide scales on these samples.

3.4 Sand Samples

Samples of sand were taken from the Howard Street Tunnel away from the proximity of the fire as well as sand that was adhered to the base of Rail #44.

[1]Dimensions scaled from WABTEC Drawing. 0592776,000,00

4 METALLURGICAL ANALYSES

Metallurgical analyses were performed on each of the samples described in Section 3. The analytical methods were selected to identify the phases present, determine the composition of the phases, and where appropriate, measure important dimensions of the components. Observed properties were compared to published properties for each of the materials, and an estimate of the thermal conditions required to produce these phase changes was derived.

4.1 Analysis Method

Sand samples collected from the Howard Street Tunnel and oxides on the steel specimens were analyzed using x-ray diffraction and Raman spectroscopy. In addition, specimens were mounted in epoxy and cross sectioned for metallurgical analyses. The cross-sectioned specimens were examined using both an optical microscope and a scanning electron microscope with an energy dispersive spectrometer.

Estimations of component temperature and fire duration were made by assessing the extent of iron oxidation and metal loss. Oxidation of iron and carbon steels is dependent on temperature. At temperatures as high as 1,600 °C [2,912 °F], both magnetite (Fe_3O_4) and hematite (α–Fe_2O_3) are stable (Rapp, 1980). Wustite ($Fe_{1-y}O$) is stable in the temperature range of 567 to 1,400 °C [1,052 to 2,552 °F]. Wustite formed at elevated temperatures is not stable at lower temperatures and is transformed to Fe + Fe_3O_4. The rate of oxidation is also dependent on temperature. At a temperature of 250 °C [482 °F] or greater, the oxide on iron and steels grows at a parabolic rate (Szlarska-Smialowska and Jurek, 1976; Runk and Kim, 1970). The thickness of the oxide scale, X, is a function of time according to Eq. (4-1)

$$X^2 = k_p t \qquad (4\text{-}1)$$

where k_p is the rate constant and t is time. A similar expression can be used to determine the metal recession rate as a consequence of oxidation (Simms and Little, 1987).

Figure 4-1 shows the rate constants for metal reduction (k_r), and scale thickness (k_p) obtained for an Fe-$2^1/_4$Cr-1Mo steel and iron. Rate constants for Fe-$2^1/_4$Cr-1Mo were reported by Simms and Little (1987) and Larose and Rapp (1997) over a temperature range from 550 to 700 °C [1,022 to 1,292 °F]. Kubaschewski and Hopkins (1962) reported rate constants for iron from 500 to 1,100 °C [932 to 2,012 °F]. The composition and microstructure of the steels are known to affect oxidation kinetics. Additions of carbon increases the oxidation kinetics of steel. Oxidation kinetics are faster for fine pearlite compared to coarse pearlite or a spheroidized microstructure (Runk and Kim, 1970). Based on data published by Kubaschewski and Hopkins, (1962) , the reduction in metal thickness as a consequence of oxidation under isothermal conditions is shown in Figure 4-2. The change in the rate of metal loss as a function of time is a result of oxide spalling. Similarly, the metal oxide thickness as a function of time and temperature can be calculated and is shown in Figure 4-3. It should be noted that the calculated values for reduction in metal thickness and oxide scale thickness shown in Figures 4-2 and 4-3 do not consider the effects of composition because the calculations are based on results observed for iron. The effect of microstructure was also not considered (Runk and Kim, 1970). Oxide cracking and spalling are assumed when the oxide scale is greater than 85 µm in thickness (Simms and Little, 1987;(Kubaschewski and Hopkins, 1962). Error in the assessment of temperature as a consequence of neglecting compositional and microstructural effects

should be considered. Increasing the carbon content of steel from 0.2 to 0.8 wt% increases the rate constant for oxide film thickness by 42 percent (Runk and Kim, 1970). Microstructure has similar effect. Runk and Kim (1970) reported the rate constant for 0.81 wt% carbon steel with a fine pearlite structure to be 52 percent greater than that for a spheroidized microstructure. Oxide film spalling is known to occur at temperatures as low as 700 °C [1,292 °F] (Kubaschewski and Hopkins, 1962). Spalling results in exposure of the underlying metal and, as a result, can significantly increase the rate of metal loss. Metal loss and oxide scale thickness shown in Figures 4-2 and 4-3 are calculated assuming that the oxidation kinetics after scale spalling are identical to a clean metal surface. It should be noted that the calculated oxide scale thickness shown in Figure 4-3 is the total oxide scale thickness which considers the change in oxidation rate as a result of spalling. The observed scale is likely to be much thinner as a consequence of sloughing after cracking and spalling.

Additional metallurgical analyses of the undamaged steel components may have been useful to assess the temperature and time of exposure. To perform these analyses, corresponding components that were not exposed to elevated temperatures are needed to assess the effects of the fire temperature and duration on microstructural changes. Because the corresponding components were not available for comparison, however, these analyses were not performed.

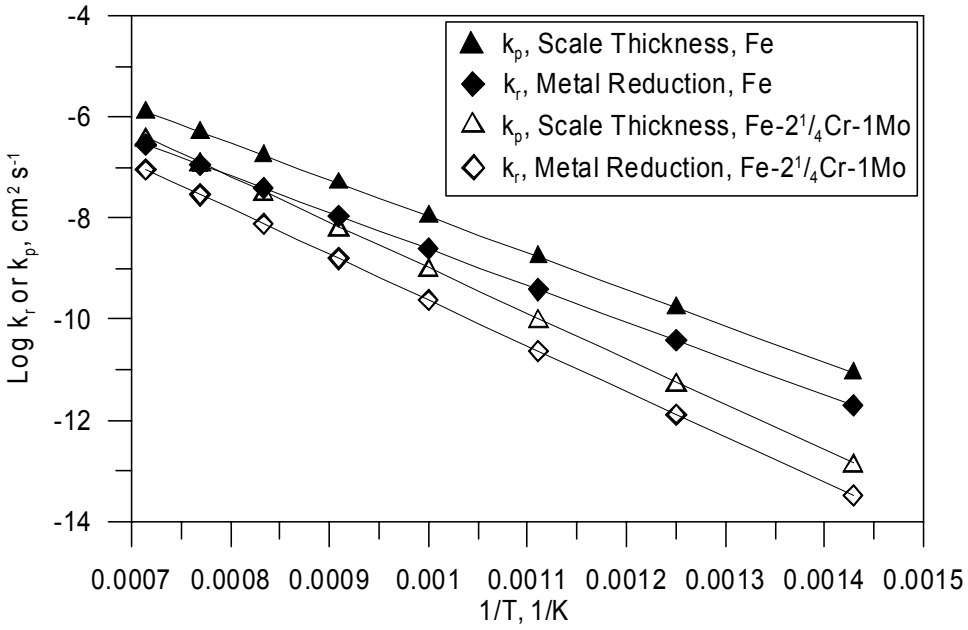

Figure 4-1. Oxidation Rate Constants for Fe-2¼Cr-1Mo Steel and Iron as a Function of Temperature (Simms and Little, 1987; Kubaschewski and Hopkins, 1962)

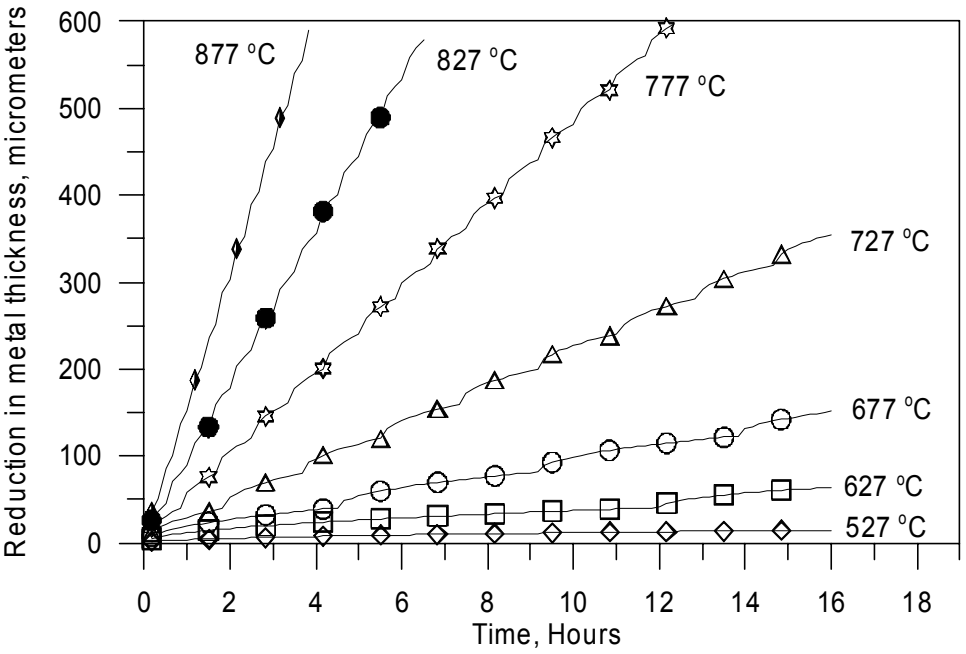

Figure 4-2. Reduction in Metal Thickness as a Function of Time for Isothermal Exposures of Iron in the Range of 527 to 877 °C [980 to 1,610 °F]

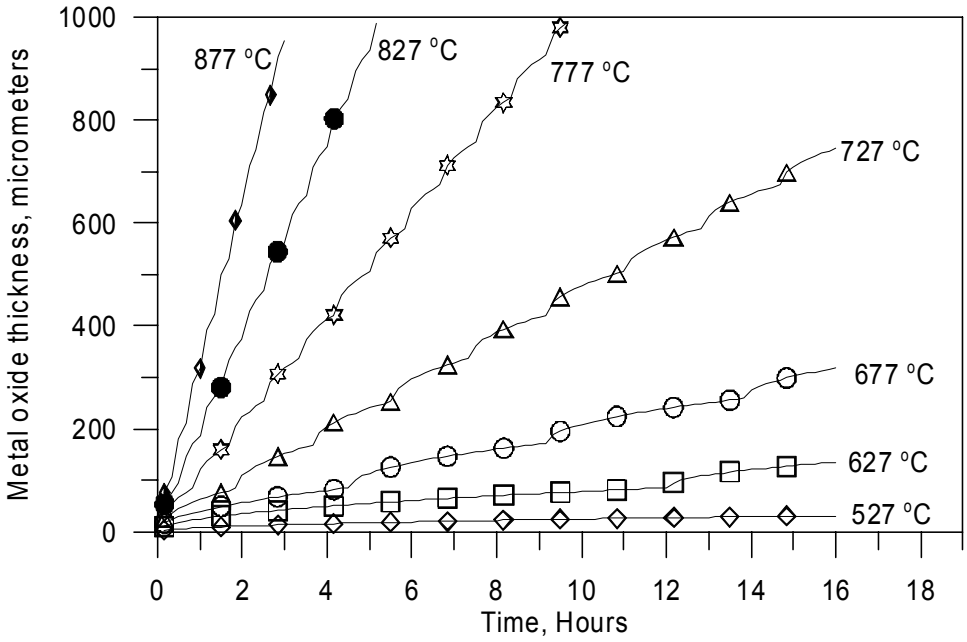

Figure 4-3. Metal Oxide Thickness as a Function of Time for Isothermal Exposures of Iron at Temperatures Ranging from 527 to 877 °C [980 to 1,610 °F]

4.2 Results

Both Raman spectroscopy (Figure 4-4) and x-ray diffraction (Figures 4-5 and 4-6) of the scale obtained from Car 51 indicate the presence of leproidocrocite (γ–FeOOH), hematite (α–Fe_2O_3) and possibly magnetite (Fe_3O_4). It should be noted that magnetite can easily be oxidized in air to hematite. The presence of γ–FeOOH, which covered large sections of the scales, indicates that the specimens were exposed to either a humid environment or water. Formation of γ–FeOOH may have occurred as a result of water contact after rupture of the water main, fire fighting efforts, or subsequent storage of the train cars involved in the derailment.

As indicated in Section 4.1, the thickness of the iron oxide scale is a function of temperature and time. Although thickness of the scales obtained from Car 51 varied, a thickness of 400 to 430 µm [0.016 to 0.017 in] was obtained by examination of the specimen cross section. Initial calculations using Eq. (4-1) and rate constants from Kubaschewski and Hopkins (1962) show that an oxide of 420 µm [0.017 in] can be formed at 777 °C [1,430 °F] in 4 hours. At 827 °C [1,520 °F], a 420-µm [0.017 in] thick scale can be produced in 2 hours.

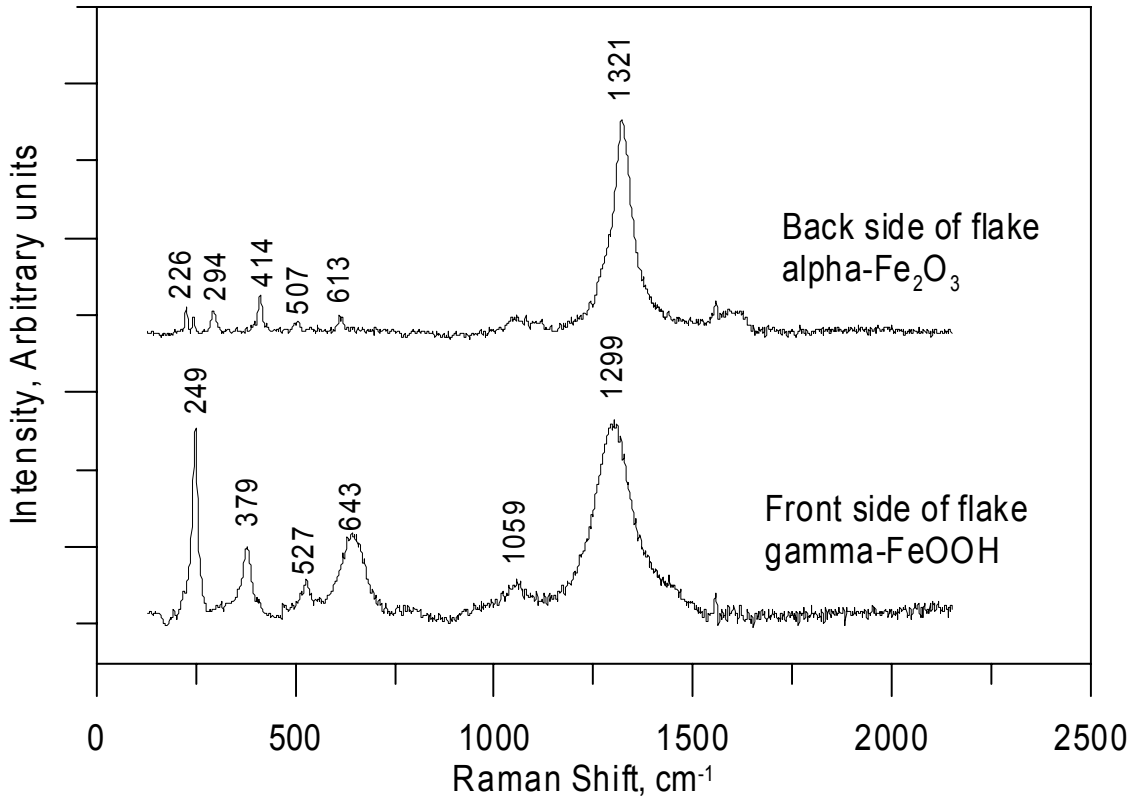

Figure 4-4. Raman Spectra for Scales Recovered from Car 51

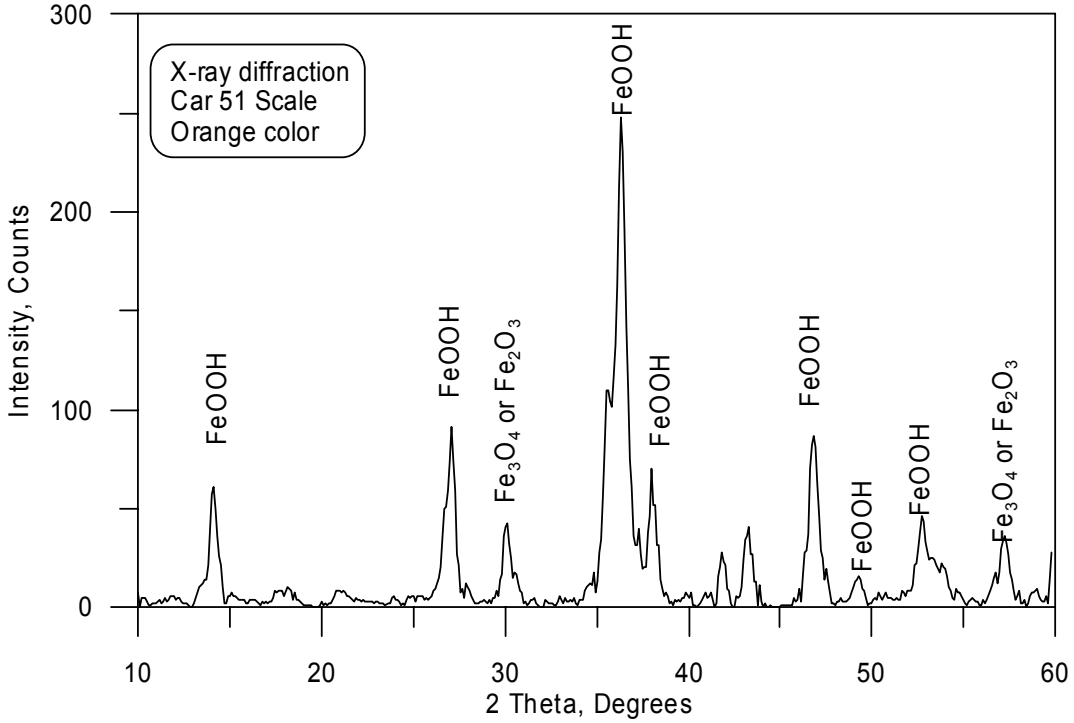

Figure 4-5. X-Ray Diffraction of Orange Colored Oxide Scales from Car 51

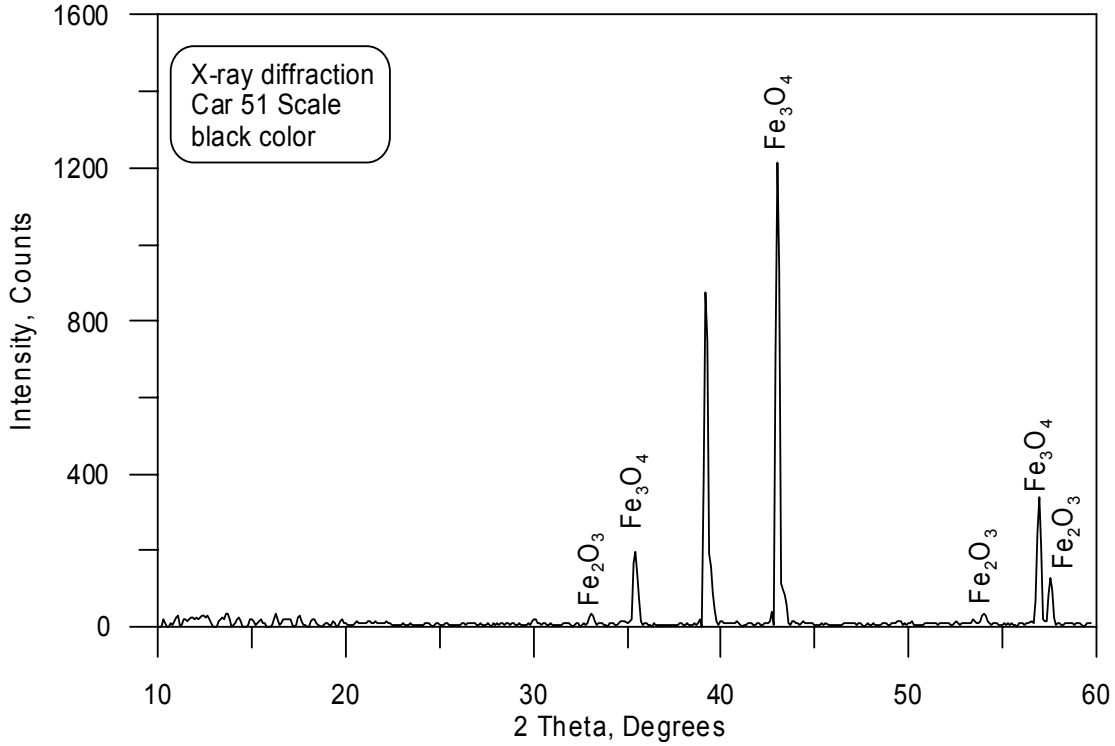

Figure 4-6. X-Ray Diffraction of Black Colored Oxide Scales from Car 51

Specimens from the roof section of Car 50 were analyzed for oxide scale thickness as well as the thickness of the remaining steel section. The first specimen was cut from the opposite end of the roof panel section that may not have been directly exposed to the fire (Figure 4-7). The second specimen was cut from the edge of the roof panel section that was directly exposed to flames from the paper inside the box car (Figures 4-8 and 4-9). From the cross section of the roof shown in Figure 4-7, the remaining metal thickness was determined to be 1,761 µm [0.069 in]. Near the edge of the roof, the metal thickness varies from 829 µm [0.033 in] at the edge (Figure 4-9), to 1,464 µm [0.058 in] at a distance approximately 3 cm [1.2 in] from the exposed edge (Figure 4-8). Although it is apparent that the metal thickness of the roof section shown in Figure 4-7 has been reduced by oxidation, the metal thickness of this section was used as a basis to determine metal loss. Assuming that metal loss occurred at equal rates on both sides of the specimen shown in Figures 4-8 and 4-9, the metal loss from each side varied from 148 to 466 µm [0.006 to 0.018 in]. Based on the calculated reduction in metal thickness as a function of time and temperature shown in Figure 4-2, temperatures in the range of 750 to 850 °C [1,382 to 1,562 °F] for approximately 4 hours would be required to achieve the reduced metal thickness.

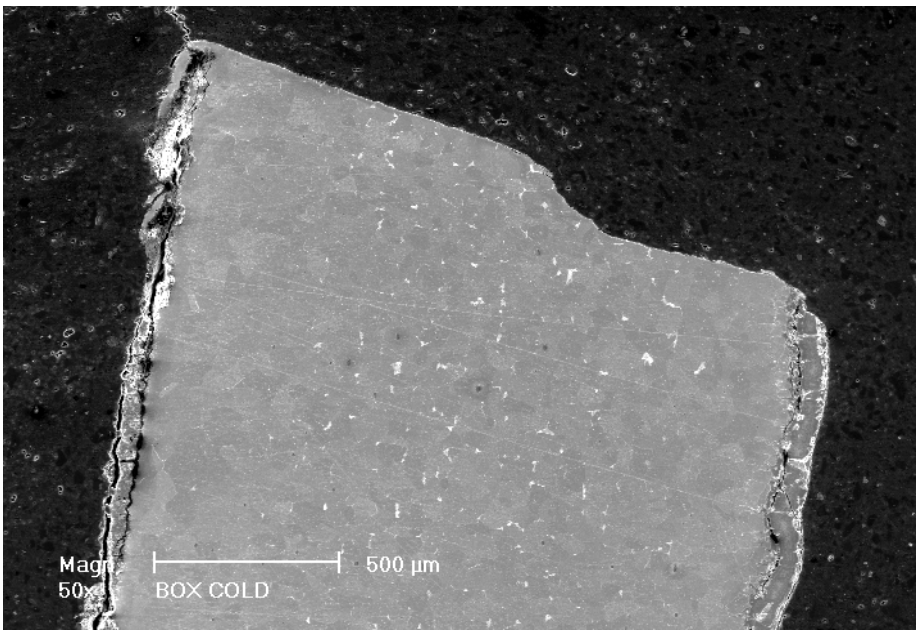

Figure 4-7. Cross section of Car 50 Roof Approximately 40 cm [16 in] from the Opposite End of the Roof Panel Section that May Not Have Been Exposed to the Fire. Thickness of the Metal was Approximately 1,761 µm [0.069 in].

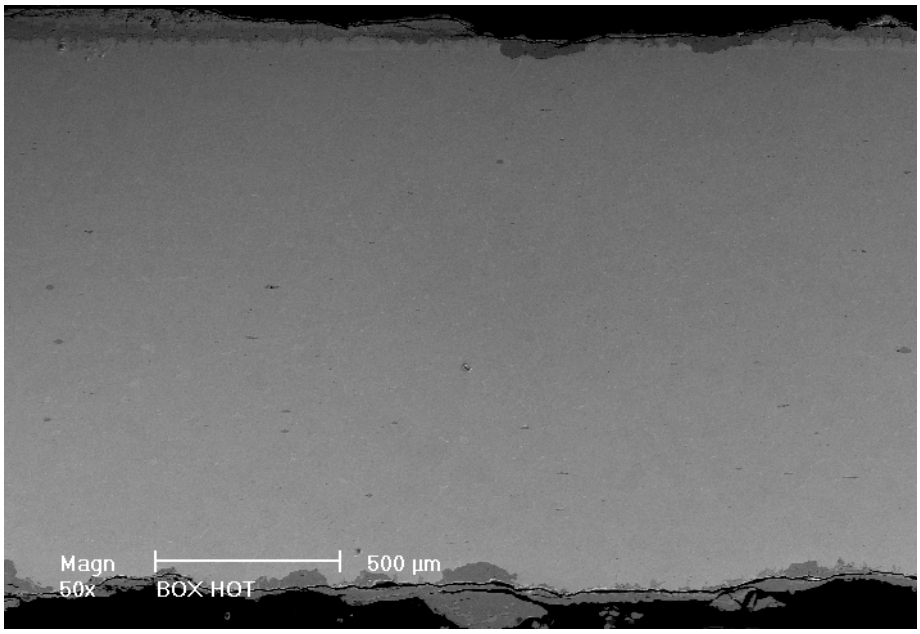

Figure 4-8. Cross Section of Car 50 Roof Approximately 3 cm [1.2 in] from the Edge Directly Exposed to the Fire. Thickness of the Metal was Approximately 1,464 µm [0.057 in].

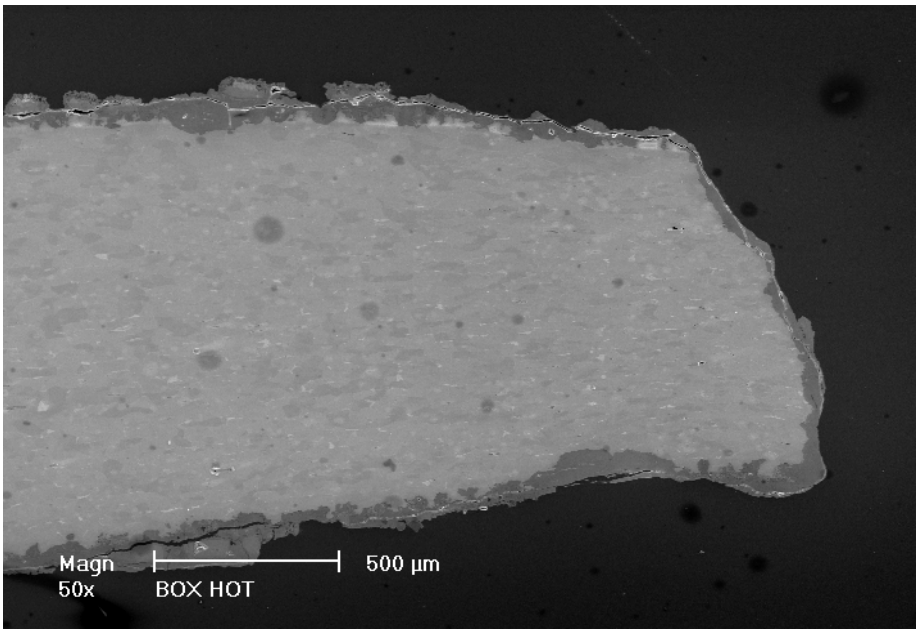

Figure 4-9. Cross Section of Car 50 Roof at Edge Directly Exposed to the Fire. Thickness of the Metal Ranged from 829 to 930 µm [0.033 to 0.037 in].

Figure 4-10(a) shows a closeup of the metal oxide scale of the Car 50 roof section near the edge exposed to the fire. Cracks and spalling of the oxide are apparent from the cross section. Figure 4-10(b) shows the scanning electron microscope-energy dispersive spectrometer element map for iron, and Figure 4-10(c) shows the element map for oxygen which confirms the scale is an iron oxide. Based on the analyses of the cross-sectioned specimen, the oxide scale on the roof section exposed to the fire ranged from 50 to 81 µm [0.0019 to 0.0032 in] in thickness. According to the calculations shown in Figure 4-3 scales of this thickness can be produced at temperatures below 700 °C [1,292 °F] for a period of 4 hours. However, the oxide scale shown in Figure 4-10(a) has clear signs of spalling which may have reduced the scale thickness that remained attached to the damaged roof section.

The cross section of the air brake bolt is shown in Figure 4-11. The oxide scale on the bolt shank was determined to be 53 µm [0.0021 in]. Little spalling or cracking of the oxide layer was observed, suggesting the temperature was less than that achieved by the roof panel of Car 50. Based on the predicted metal oxide thickness shown in Figure 4-3, a 53 µm [0.0021 in] oxide scale could be expected in 4 hours at 627 °C [1,160 °F]. At higher temperatures, spalling of the oxide would be expected.

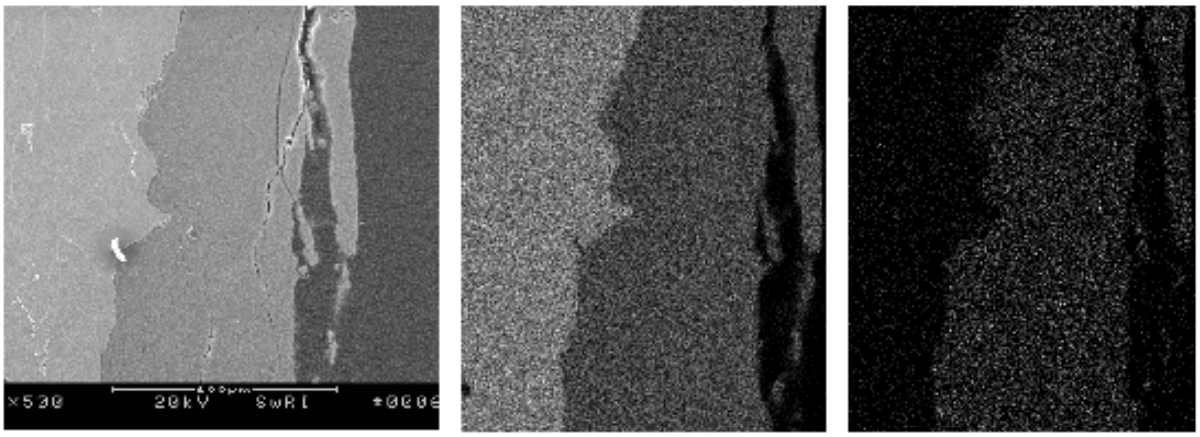

Figure 4-10. (a) Secondary Electron Image from Car 50 Roof at Edge Directly Exposed to the Fire, (b) Iron Image Map, (c) Oxygen Image Map

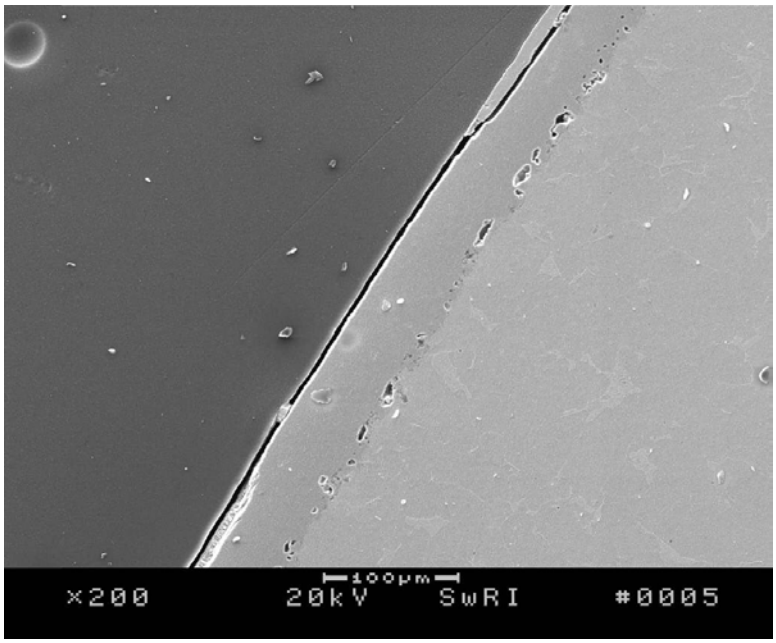

Figure 4-11. Scanning Electron Microscope Secondary Electron Image of Car 52 Air Brake Valve Bolt Showing Metal and Oxide Layer

Figure 4-12(a) shows a cross section of one of the air brake assembly bolts. During the analysis of the specimen, several regions were found where an aluminum–iron phase had formed. A higher magnification of such a region is shown in Figure 4-12(b). Using an energy dispersive spectrometer, the composition of the bolt was determined to be 98.4 atomic percent iron with no measurable concentration of aluminum. In the mixed aluminum–iron region, the composition was found to be 66 atomic percent aluminum, 4 atomic percent silicon, and 30 atomic percent iron. The liquidus temperature for a 66 atomic percent Aluminum and 34 atomic percent iron binary is 1,180 °C [2,156 °F] and the solidus temperature is 1,165 °C [2,129 °F] (ASM International, 1992). The aluminum–iron binary phase diagram does not contain low melting point eutectic compositions. The addition of 4 atomic percent silicon is not expected to significantly alter the solidus or liquidus temperatures based on examination of the iron–silicon and aluminum–silicon binary systems.

The aluminum–iron phase identified on the air brake valve bolt may have been formed as a result of diffusion of aluminum into the iron at elevated temperatures. Eq. (4-2) describes simple diffusion

$$x = \sqrt{Dt} \tag{4-2}$$

where x is the diffusion distance (cm) [in], D is the diffusion coefficient ($cm^2\ s^{-1}$) [$in^2\ s^{-1}$] and t is time (seconds). Assuming a diffusion distance of 100 µm [0.0039 in] and a time of 10 hours, the calculated value of D is 2.8×10^{-9} $cm^2\ s^{-1}$ [4.3×10^{-10} $in^2\ s^{-1}$]. The value of D is dependent on temperature. For face center cubic iron (γ-Fe), a self-diffusion coefficient of 2.8×10^{-9} $cm^2\ s^{-1}$ [4.3×10^{-10} $in^2\ s^{-1}$] corresponds to a temperature of 1,464 °C [2,667 °F] (Geiger and Poirier, 1980).

The sand samples were identified as quartz (SiO_2) using Raman spectroscopy. Results of x-ray diffraction analyses also indicated quartz and small amounts of ankerite [$Ca(Fe,Mg)(CO_3)_2$]. The sample obtained from Rail #44 also had Raman peaks consistent with the presence of γ–FeOOH. As previously indicated, the presence of γ–FeOOH is consistent with corrosion of iron and steel rather than oxidation at elevated temperatures.

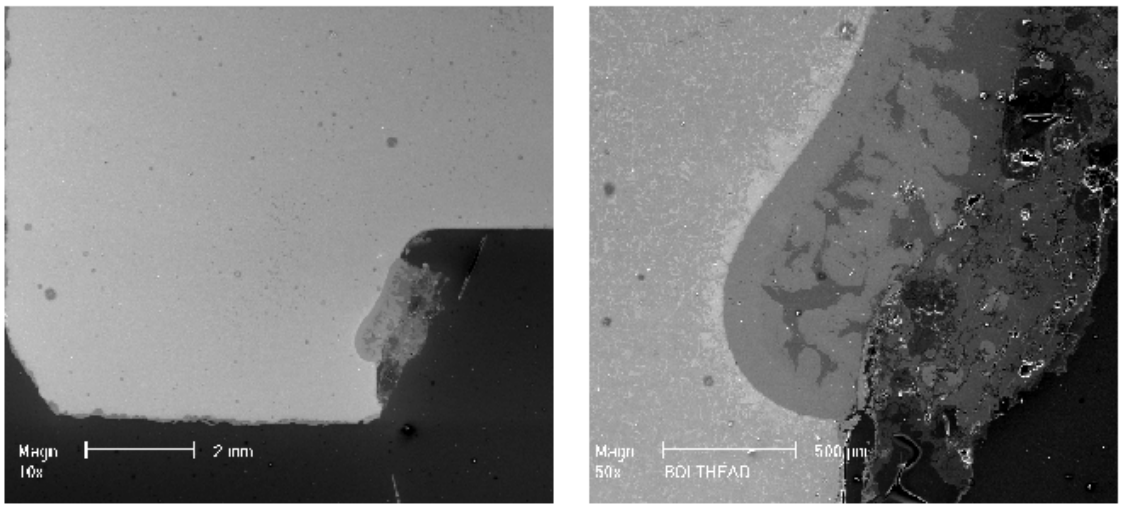

Figure 4-12. (a) Scanning Electron Microscope Secondary Electron Image of Car 52 Air Brake Valve Bolt Head Showing Iron and Aluminum and (b) Closeup of Iron with Aluminum

4.3 Discussion

Analyses of the scale obtained from Car 51 suggest the oxide was initially formed as a result of high-temperature oxidation. Subsequent exposure to water or humid air resulted in the formation of iron hydroxides that are typical of corrosion products for steel structures exposed to a humid or aqueous environment. Calculations of the time and temperature required to form oxide scales of similar in thickness to the specimens obtained from Car 51 or from the roof of Car 50 do not consider changes in thickness that may result from subsequent exposure to humidity or water.

The thickness of the oxide scales recovered from Car 51 and the reduced metal thickness observed in the roof panel of Car 50 correspond to temperatures in the range of 750 to 850°C [1,382 to 1,562 °F]] for a period of approximately 4 hours. The estimation of the temperature does not consider the effects of steel composition and microstructure (Runk and Kim, 1970; Hauffe, 1965) or the partial pressure of oxygen (Kubaschewski and Hopkins, 1962) on the oxidation kinetics. Cross sections of the roof panel from Car 50 clearly indicate significant cracking of the oxide, suggesting the roof panel reached temperatures where spalling of the oxide may be expected. Cracks in the oxide scales tend to increase the oxidation rate of the underlying metal. Assessment of the oxide layer thickness is compromised by scale thickness variation and scale spalling. As a result, assessments of the temperature of the component and fire duration using the thickness of the oxide scales may have significant errors.

Estimations of component temperature and fire duration from the analysis of the oxide scale thickness and the reduction in the metal thickness are dependent on the selection of kinetic parameters. As indicated in Section 4.1, the rate constants are dependent on several factors, including microstructure and composition. Additional calculations were performed to determine the effects of uncertainty in the values of the rate constants. Multiplying the rate constants shown in Figure 4-1 by a factor of 2 increased the oxide scale or reduced metal thickness by approximately 50 percent.

Spalling of the oxide may also be problematic for the assessment of temperature because of uncertainty in the conditions necessary for spalling to occur and the uncertainty in the oxidation rates after spalling of the oxide scale. On the other hand, the adhesion of iron oxides to iron is a function of temperature and scale thickness (Kubaschewski and Hopkins, 1962) and may provide a marker for the temperature achieved by the steel components. For scales of 200 µm [0.0079 in] thickness, the adhesion increases as temperature increases from 650 to 775 °C [1,202 to 1,427 °F] and then decreases to zero at 950 °C [1,742 °F]. When the adhesion strength decreases, the oxide can be easily removed from the metal, and spalling can occur. Spalling of oxide scales on iron and steel is generally observed at temperatures of 850 °C [1,562 °F] but has been observed as low as 700 °C [1,292 °F] (Kubaschewski and Hopkins, 1962). The scale recovered from the brake end of Car 51 adjacent to Car 52 was completely separated from the underlying steel, suggesting the steel reached temperatures above 700 °C [1,292 °F].

The oxide scale on the bolt recovered from the air brake valve of Car 50 appeared to be more intact than the scale on the roof panel of Car 50, suggesting that the oxide on the bolt was formed at a lower temperature. The observation of the aluminum–iron–silicon phase on the underside of the bolt head is inconsistent with the lower component temperature suggested by the intact, 53-µm [0.0021-in] thick oxide scale on the shank of the bolt. It is unlikely that the

formation of aluminum–iron–silicon occurred as a result of diffusion of aluminum into the steel bolt. No low melting point eutectic exists in the aluminum–iron, aluminum–silicon, or the iron–silicon systems that would result in the formation of this phase.

Initial analyses of the sand collected from the tunnel did not provide a means to estimate temperature. Quartz has a melting temperature of 1,610 °C [2,930 °F], which is greater than the solidus temperature of carbon steel. Although not completely conclusive, the x-ray diffraction analyses indicated the presence of ankerite, which contains carbonate. Carbonate minerals tend to decompose and evolve carbon dioxide at elevated temperatures. Specific information on ankerite was not available but ankerite is similar to dolomite [$CaCO_3 \cdot MgCO_3$], which decomposes at temperatures above 730 °C [1,346 °F]. Because ankerite appears to be present in both sand samples collected at locations close to and away from the fire, it appears that the sand collected from Rail #44 did not achieve temperatures in excess of 730 °C [1,346 °F].

5 ALUMINUM SAMPLE THERMAL MODEL

A fundamental heat transfer analysis of the aluminum air brake cover found on Car 51 was conducted. The procedure followed is commonly used to predict the length of exposure required to bring a structural element to a critical temperature and the failure times in steel sections, based on strength reductions at elevated temperatures.

5.1 Assumptions

To simplify our initial analysis, the following assumptions were made:

Lumped Mass—The aluminum components were assumed to be lumped masses of solid aluminum. It is also assumed that the temperature of the relatively small volume of aluminum is uniform. This assumption is conservative because it will over predict the amount of aluminum present for phase change.

Full Volume of Aluminum—In the absence of an accurate values of aluminum volume contained in the valve cover, a calculation of the volume of the cover was made based on dimensions provided in WABTEC drawings. This assumption is conservative because it will predict higher temperatures to cause melting of the larger volume.

Complete Melting—The aluminum section reached its liquidus temperature. This is a good assumption considering the condition of the covers in Figure 3-2.

Zero Conductive Losses to Adjacent Valve—This analysis considers the aluminum portion separate from any adjacent material. This condition will predict slightly faster melting times than the actual case, which is, however, a fair assumption when the cover deforms and drips away from the main valve assembly.

Convective Heat Transfer Coefficient—The heat transfer coefficient was assumed to be 50 kW/m²K. This value was taken from the Eurocode, as referenced in Buchanan (2001). This heat-transfer coefficient is suggested when calculating the exposure of steel elements in a hydrocarbon fire. According to Buchanan, heat transfer is not strongly heat-transfer coefficient dependent because the primary heat-transfer mode is radiation.

Flame Temperature—A common flame temperature for a typical hydrocarbon fuel is between 810 and 925 °C [1,490 and 1,697 °F] (DeHaan, 1991). The analysis utilized two types of ramp functions; ramp to a maximum temperature and plateau; and ramp-plateau-decay temperature profiles. The ramp-plateau decay fire profile most accurately represents the conditions in the tunnel because of the ventilation constraints of the tunnel geometry. Results for ramp-plateau and ramp-plateau-decay functions are presented in Section 5.4.

Radiative Exposure—The added exposure because of radiation from the luminous flame was not considered. The radiative fraction is typically taken to be approximately 30 percent of the total heat release of the burning fuel. This fraction changes with changes in oxygen availability and burning efficiency of the fuel. Appropriate values for radiant exposures range between 20 and 50 kW/m². These values were chosen based on published radiative fractions of known hydrocarbons (Tewarson, 1995; Drysdale, 1985). The exclusion of radiative inputs will lead to longer predicted exposure times.

5.2 Basic Equations

The analysis is based on the principle that heat entering the aluminum section over a period of time (Δt) raises the temperature by some amount (ΔT). This concept is represented as

$$\dot{q}'' \bullet F \Delta t = \rho_{Al} \bullet c_{Al} \bullet V \bullet \Delta T_{Al} \tag{5-2}$$

where

$$\dot{q}'' = h_c\left(T_f - T_{Al}\right) + \sigma \varepsilon \left(T_f^4 - T_{Al}^4\right) \tag{5-3}$$

Substituting Eq. (5-2) into Eq.(5-1) yields:

$$\Delta T_s = \frac{F}{V} \bullet \frac{1}{\rho_s c_s} \left\{ h_c\left(T_f - T_{Al}\right) + \sigma \bullet \varepsilon \left(T_f^4 - T_{Al}^4\right) \right\} \Delta t \tag{5-4}$$

where

ΔT_{Al}	—	Change in aluminum temperature (K)
F	—	Surface area (m²)
V	—	Volume (m³)
ρ	—	Density of aluminum (2,707 kg/m³)
c_{Al}	—	Specific heat of aluminum (0.892 kJ/kgK)
h_c	—	Heat transfer coefficient (50 W/m²K)
T_f	—	Flame temperature (K)
T_{al}	—	Aluminum temperature (K)
σ	—	Stefan-Boltzman constant (56.7×10^{-12} kW/m²K⁴)

Emissivity (ε) is given by

$$\varepsilon = \frac{1}{\left[\left(\frac{1}{\varepsilon_S} + \frac{1}{\varepsilon_R}\right) - 1\right]} \tag{5-5}$$

where

ε_S	—	Emissivity of the source
ε_R	—	Emissivity of the receiver

Emissivities were assumed to be 0.67 for both the emitter and the receiver (Buchanan, 2001).

5.3 Analysis Method

A timestep (Δt) was chosen, and the equations were solved to provide the ΔT at each timestep. A Microsoft® VisualBasic program was used for the repetitive calculations. A brief sensitivity analysis was performed on h_c and ε, because these two variables are easily changed (as opposed to the material property variables).

Two temperature functions were tested, as described in Section 5.1. The analysis focused on ramp-plateau and ramp-plateau-decay temperature profiles. Standard values for nonene (or similar hydrocarbon fuels) indicate a flame temperature between 810 and 925 ˚C [1,697 ˚F]. These values were used as starting points for the thermal analysis. Where possible, data obtained from metallurgical analyses were used to further adjust the temperature profile.

5.4 Results

Preliminary model results for several possible fire scenarios are provided. All the results presented assume the same sample geometry, material properties, and heat transfer coefficients. The constant inputs are provided in Sections 3.1 and 5.1. Fire temperature profiles were varied and predicted aluminum profile performance was noted.

5.4.1 Ramp-Plateau Function

The ramp-plateau function assumed the maximum temperature was realized in 3 minutes, and was maintained for the duration of the exposure. This ramp function is typical of hydrocarbon fires modeled in test furnaces. The American Society for Testing and Materials (1993) suggests a temperature of 1,093 ˚C for 3 minutes and 1,180 ˚C [2,156] for 5 minutes, and all times thereafter. This is a very conservative assumption considering the limited availability of fuel (based on spill rate) and the limited supply of oxygen for combustion (based on tunnel geometry).

When modeled using this fire exposure, the sample aluminum element exhibits melting at 300 seconds into the exposure (see Figure 5-1).

A more realistic ramp function would use the upper and lower bound for flame temperature, as found in the literature. These temperatures are 810 and 925 ˚C [1,490 and 1,697 ˚F], respectively. These exposure conditions predict melting at approximately 500 seconds.

Both of these models predict the aluminum melted before a reasonable fire duration could be obtained.

Figure 5-2 illustrates that, when taking the published flame temperature as the maximum temperature experienced by the valve, any exposure time greater than 360 seconds will produce melting conditions.

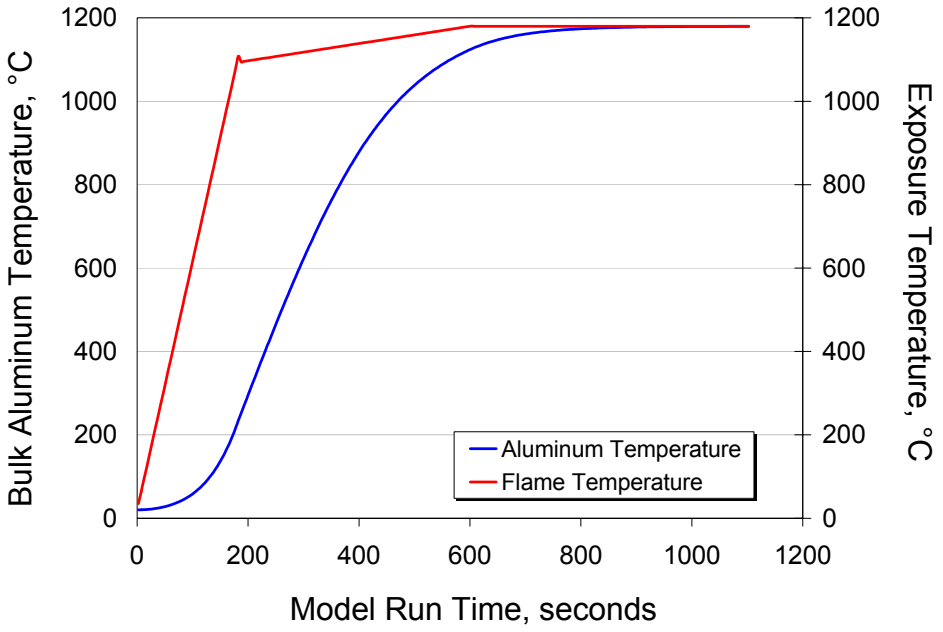

Figure 5-1. ASTM E 1529 (1993) Ramp Function and Corresponding Aluminum Thermal Profile (Melting Predicted at 300 seconds)

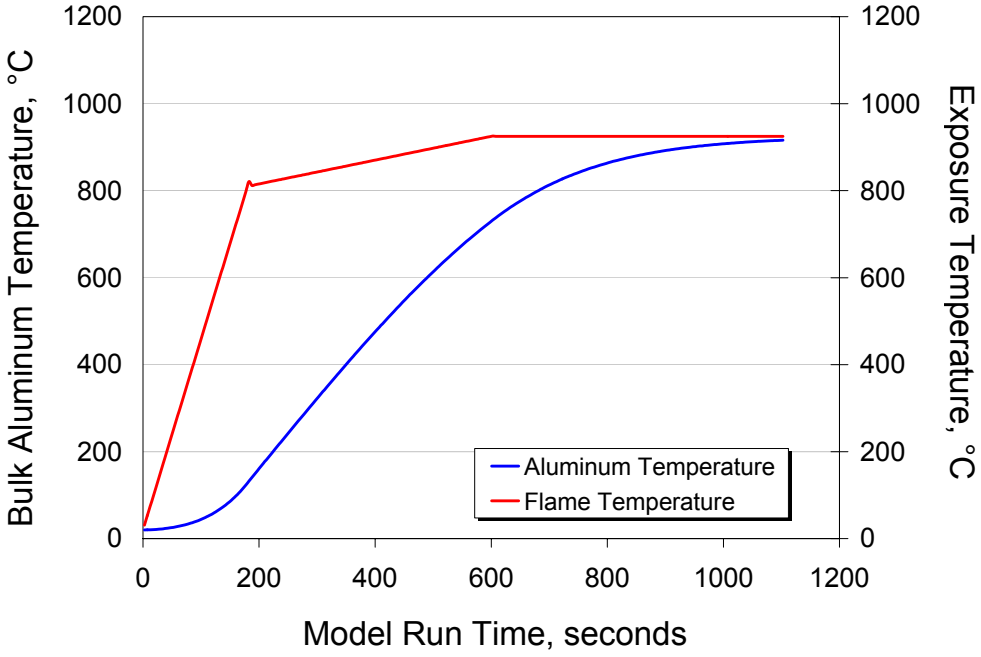

Figure 5-2. Published Flame Temperature Ramp Function and Corresponding Aluminum Thermal Profile (Melting Predicted at ~500 seconds)

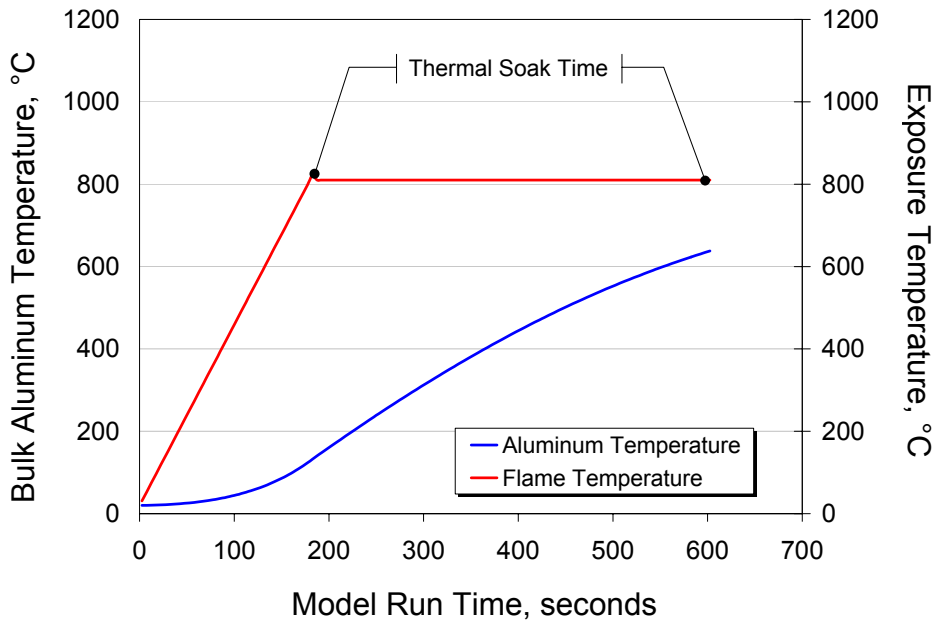

Figure 5-3. Ramp-Plateau Function Demonstrates Melting at Published Flame Temperature for Exposure Times Greater than 360 Seconds

5.4.2 Ramp-Plateau-Decay Function

A more realistic approach is to take into account a slower growth rate and the decay in flame temperature as oxygen becomes scarce in the tunnel. Flammable liquids burning in pool fires, in open air, can be expected to provide temperature profiles consistent with Figures 5-2 and 5-3. Fires burning under limited oxygen conditions will decay following the initial rise and stabilize at some equilibrium temperature until ventilation conditions change or fuel is exhausted. It is also safe to assume the temperatures at the valve {roughly 10 m [33 ft] from the source} would have taken longer to reach the flame temperature. According to ASTM E 1529 (1993), a 3-minute ramp will completely immerse an element in an open-burning fire. A 7.5-minute initial ramp was chosen here. A decay to half the fire temperature was assumed to have occurred 18 minutes into the fire exposure (assuming oxygen starvation).

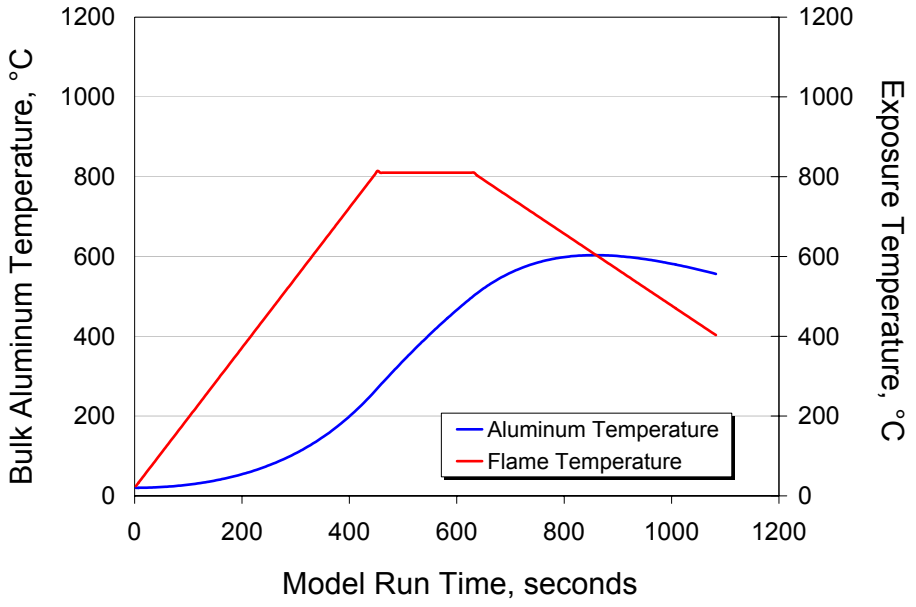

Figure 5-4. Ramp-Plateau-Decay Function and Corresponding Aluminum Thermal Profile (Melting Predicted at ~800 seconds)

The conditions depicted in Figure 5-4 may be more difficult than originally assumed because 810 ˚C [1,490 ˚F] is the actual, published flame temperature of the fuel. The valve would have had to be completely engulfed in flames for it to realize these temperatures. Considering the location of the value, 10 m [33 ft] uphill, and its position in the tunnel (low to the floor), total flame engulfment may have only occurred intermittently and, possibly, for only a short duration.

5.5 Discussion

The model was run with several variations in h_c and ε. In all cases, the model predicted the melting occurred between 793 seconds (assuming h_c = 25 W/m²K and ε = 0.26) and 463 seconds (assuming h_c = 50 W/m²K and ε = 0.5). The predictions of melting at far less than 1,800 seconds could not be used to ascertain the duration of the exposure.

Even when not considering the radiative exposure of the sample to the flame luminosity, the melting time of the valve cover is predicted to have occurred early in the exposure. Considering the radiative inputs would have considerably decreased the melting time. In relation to laboratory testing, in order to simulate a radiative heat flux of 50 kW/m², samples are exposed to a furnace environment of approximately 800 °C [1,472 ˚F].

Had the model predicted melting at over 1,800 seconds, one could deduce the fire duration was at least 1,800 seconds. The data indicated the aluminum section melted very early in the fire duration and the aluminum was severely damaged as a result of the fire exposure before the aluminum performance could be used to establish fire duration.

6 CONCLUSIONS

Metallurgical analyses were conducted to assess the fire temperature and fire duration. The analyses were partially confounded by several factors including the atmospheric exposure of the rail car components for a period of more than 1 year following the fire. Another limitation of the analyses was the lack of suitable controls, or components that were not exposed to the fire, that could be used to assess extent of fire damage to the recovered components. Metallurgical analyses suggest that the fire temperature at the end of Car 51, adjacent to Car 52, was at least 700 ˚C [1,292 ˚F] and likely closer to 850 ˚C [1,562 ˚F], based on the observation of spalling of the oxide scale. Based on the reduction in the thickness of the roof of Car 50, temperatures for this component were estimated to be in the range of 750 to 850 ˚C [1,382 to1,562 ˚F] for a period of 4 hours. The oxide formed on the steel bolt from the air brake valve assembly of Car 52 suggests the temperature in this region was estimated to be 627 ˚C [1,160 ˚F] for an exposure period of 4 hours.

The preliminary data reviewed, including a first-look metallurgical analysis coupled with a simplified thermal model, indicate conditions causing melting in the aluminum could only occur if temperatures in excess of 600 ˚C [1,112 ˚F] were achieved in the sample, for an appreciable duration.

A second aluminum witness was found approximately 20 m [66 ft] uphill of the fire source. This piece is shown in Figure 6-1. It is interesting to note that this piece did not melt completely, which would indicate the very specific conditions required to melt the valve assembly on Car 52 were likely not encountered at approximately 20m [66 ft] away.

Figure 6-1. Air Brake Valve Found 20+ m [66 ft] from Fuel Spill Site (Note Only Partial Melting at This Location)

Closer analysis of the damage caused to the valve cover found at Car 52, indicates that a separation distance of approximately 20 m [66 ft] was sufficient to limit the exposure conditions in this area, as evidenced by the level of damage to the valve cover. Considering only partial

melting in this area, temperatures at the surface of the aluminum were only slightly above 600˚C [1,112˚F] (enough to initiate melting) but were not maintained for any appreciable duration.

A third valve, of similar construction to the valves found on Cars 51 and 52, was also found on Car 53 (approximately 40 m [downhill] from the tripropylene spill point). This valve exhibited no signs of damage at all, and was found completely intact. Thus, at separation distances of 40 m or greater, the exposure conditions were demonstrated to be less than 600˚C.

The exposure profile derived from the post-fire condition of a number of aluminum valve covers is further supported when one considers other damage noted on the railcars. Railcars (e.g. Cars 50 and 51) were painted with Dupont paint No. 909M-22416, an air-dried, high solid, alkyd-enamel paint. Given the observed damage to the steel and paint on Cars 51, 52, and 53, the blistering temperature of 700 ˚C was only realized within 15 m of the spill site. These distances were measured from the tops of the railcars (worst case), where both heat and corrosive products of combustion were concentrated. There was no damage to the paint or steel on Car 53, adjacent to the fuel spill car (52), and located 12 m from the spill site.

The exposure conditions of standard compliance tests are based on a diesel, or similar hydrocarbon, pool fire burning in an open pool configuration. For testing purposes, this fire scenario provides exposure temperatures of approximately 800 ˚C [1,472 ˚F] for 30 minutes. It is also assumed in this scenario the item being tested is in close proximity to the fuel spill source and is completely immersed in the fire environment. Administrative controls can ensure conditions that would limit the proximity of fuel sources to important cargo. The data obtained during this review of the Baltimore Tunnel Fire indicate the separation of cargo from potential fuel sources will be an acceptable method of limiting their exposure.

7 REFERENCES

ASM International. *ASM Handbook Volume 3: Alloy Phase Diagrams.* Materials Park, Ohio: ASM International. 1992.

ASTM. "Standard Test Methods for Determining Effects of Large Hydrocarbon Pool Fires on Structural Member and Assemblies." ASTM E 1529–93. 1993.

Buchanan, A.H. *Structural Design for Fire Safety.* West Sussex, England: John Wiley and Sons, Limited. 2001.

DeHaan, J.D. *Kirk's Fire Investigation—3rd Edition.* Englewood Cliffs, New Jersey: Brady—A Prentice Hall Division. 1991.

Drysdale, D. An Introduction to Fire Dynamics. New York City, New York: John Wiley and Sons, Limited. 1985

Geiger, G.H. and D.R. Poirier. *Transport Phenomena in Metallurgy.* Reading, Massachusetts Addison-Wesley Publishing Company. 1980.

Hauffe, K. *Oxidation of Metals.* New York City, New York: Plenum Press. 1965

Holman, J.P. *Heat Transfer—7th Edition.* New York City, New York: McGraw-Hill, Inc. 1990.

Kubaschewski, O. and B.E. Hopkins. *Oxidation of Metals and Alloys.* New York City, New York: Academic Press Inc. 1962.

Larose, S. and R.A. Rapp. "Review of Low Temperature Oxidation of Carbon Steels and Low Alloy Steels for Use as High-Level Radioactive Waste Package Materials." CNWRA 97-003. San Antonio, Texas: Center for Nuclear Waste Regulatory Analyses. 1997.

Rapp, R.A. *High Temperature Corrosion* (Reference Manual for Audio Course). Washington, DC: The American Chemical Society. 1980.

Runk R.B. and H.J. Kim. "The Oxidation of Iron-Carbon Alloys at Low Temperatures." *Oxidation of Metals.* Vol. 2, No. 3. p. 285. 1970.

Simms, N.J. and J.A. Little. "High-Temperature Oxidation of Fe-$2^1/_4$Cr-1Mo in Oxygen." *Oxidation of Metals.* Vol. 27, Nos. 5/6. p. 283. 1987.

Szlarska-Smialowska Z. and J. Jurek. "Ellipsometric Studies on Iron Oxide Film Growth at 100–350 °C." *Corrosion.* Vol. 32, No. 7. p. 294. 1976.

Tewarson, A. *Generation of Heat and Chemical Compounds in Fires—Society of Fire Protection Engineers (SFPE) Handbook.* Section 3, Chapter 4. pp. 3-99–100. Quincy, Massachusetts: National Fire Protection Association. 1995.